Available online at www.sciencedirect.com

SciVerse ScienceDirect

Geochimica et Cosmochimica Acta 90 (2012) 242–264

Geochimica et Cosmochimica Acta

www.elsevier.com/locate/gca

Primordial oxygen isotope reservoirs of the solar nebula recorded in chondrules in Acfer 094 carbonaceous chondrite

Takayuki Ushikubo [a,*], Makoto Kimura [b], Noriko T. Kita [a], John W. Valley [a]

[a] *WiscSIMS, Department of Geoscience, University of Wisconsin, Madison, WI 53706, USA*
[b] *Faculty of Science, Ibaraki University, Mito, Ibaraki 310-8512, Japan*

Received 23 June 2011; accepted in revised form 4 May 2012; available online 16 May 2012

Abstract

Highly precise and accurate ion microprobe analyses of oxygen three-isotope ratios in chondrules from the Acfer 094, one of the most primitive carbonaceous chondrites, show that chondrules preserve evidence for oxygen isotope heterogeneity in chondrule-forming regions of the solar nebula. Identical $\Delta^{17}O$ values in most minerals and glass within each chondrule indicate that the oxygen isotope ratio in chondrule melt did not change during or after crystallization. Nearly half of the chondrules studied contain small amounts of olivine grains that have an oxygen isotope anomaly relative to other minerals and glass in the same chondrule. Most chondrules in Acfer 094 can be classified into two oxygen isotope groups ($\Delta^{17}O \sim -2‰$ and $\Delta^{17}O \sim -5‰$) indicating that the final melting of chondrules occurred within two distinct oxygen isotope reservoirs, probably representing the local protoplanetary disk immediately before planetesimal formation. One of these reservoirs ($\Delta^{17}O \sim -2‰$) is observed from chondrules in other carbonaceous chondrites and from crystalline silicates in comet Wild 2, suggesting that crystalline silicates formed in an oxygen isotope reservoir of $\Delta^{17}O \sim -2‰$ were widely distributed in the outer asteroid belt and throughout the outer solar nebula. Oxygen three-isotope ratios of minerals in chondrules from Acfer 094 are distributed along a newly defined Primitive Chondrule Minerals (PCM) line, which has slope ~ 1 [$\delta^{17}O = (0.987 \pm 0.013) \times \delta^{18}O - (2.70 \pm 0.11)$] and intersects the terrestrial fractionation line at $\delta^{18}O = 5.8 \pm 0.4‰$. These data are distinct from, and plot between, the CCAM, and Young and Russell lines. The PCM line is interpreted to represent the mixing trend of extreme oxygen isotope reservoirs in the early solar system that were the primary oxygen isotope reservoir of solids that accreted to form planets including the Earth.

1. INTRODUCTION

Chondrules are abundant igneous silicate spherules in chondritic meteorites and are considered to form by transient high temperature processes in the solar nebula (Connolly and Love, 1998), which postdate the oldest Ca, Al-rich inclusions (CAIs) by at least 1–2 million years (Kita et al., 2005) and probably formed in a dust-enriched part of the solar nebula (Alexander et al., 2008). The recent discovery of chondrule-like objects in the short-period comet Wild 2 (McKeegan et al., 2006; Nakamura et al., 2008) indicates that chondrules were widely distributed from the asteroid belt to the Kuiper belt. Thus, both the formation processes and the migration mechanisms of chondrules in the early solar system provide critical information to understand the growth of the solar system (Ciesla, 2005).

Although bulk oxygen isotope ratios of individual chondrules are variable typically at the level of a few to several ‰, bulk chondrule data from different classes of chondrites distribute at the specific locations in the oxygen three-isotope diagram near those of their host meteorites (Clayton et al., 1983; Clayton 2003). These data have been interpreted to indicate a close relation between the regions where chondrules formed and where they accreted to make asteroidal parent bodies. In contrast, *in situ* oxygen isotope studies of chondrules using ion microprobes show that significantly

* Corresponding author. Tel.: +1 608 265 2601.
E-mail address: ushi@geology.wisc.edu (T. Ushikubo).

0016-7037/$ - see front matter © 2012 Elsevier Ltd. All rights reserved.
http://dx.doi.org/10.1016/j.gca.2012.05.010

large internal oxygen isotope variations in some chondrules are typically found in forsteritic olivine grains (Yurimoto and Wasson, 2002; Jones et al., 2004; Kunihiro et al., 2004, 2005; Kita et al., 2010). In some cases, both $\delta^{18}O$ and $\delta^{17}O$ values are as low as $-50‰$, suggesting a close relation with a ^{16}O-rich component observed in the CAIs ($\delta^{18}O \sim \delta^{17}O \sim -45‰$, e.g., Clayton, 2003), an unusual chondrule from CH chondrite ($\delta^{18}O \sim \delta^{17}O \sim -75‰$, Kobayashi et al., 2003), and the solar wind ($\delta^{18}O \sim \delta^{17}O \sim -59‰$ for the Solar Wind L1 point, McKeegan et al., 2011), which may represent the initial solar system oxygen isotope ratios (Clayton, 2002; Yurimoto and Kuramoto 2004). Therefore, precursors of chondrules might be derived from various sources with distinct oxygen isotope ratios that partly survived in chondrules in primitive meteorites.

Oxygen isotope ratios of many chondrules from carbonaceous chondrites indicate that chondrules record partial exchange of oxygen between the chondrule-forming melt and ambient gas that was ^{16}O-poor relative to chondrule precursors (Clayton et al., 1983; Bridges et al., 1999). This conclusion is supported by values of glass that are systematically higher in $\delta^{18}O$ and $\delta^{17}O$ relative to olivine and pyroxene phenocrysts in the same chondrule (Bridges et al., 1999; Chaussidon et al., 2008). However, based on recent oxygen isotope analyses of chondrules in Semarkona, Kita et al. (2010) suggested that oxygen isotope ratios in chondrule glass would have been partially altered by fluids in the parent body. Furthermore, if chondrule formation occurred in a dust-rich environment by shock-wave heating (Alexander et al., 2008), the oxygen isotope ratios of the ambient gas might be dominated by that of chondrule precursors. In this case, the oxygen isotope ratios of ambient gas are expected to have approached the average oxygen isotope ratios of chondrule precursors, which would be recorded in chondrule-forming melt. Existence of the ^{16}O-poor primordial dust in the Solar Nebula has been discussed by Krot et al. (2010).

To understand the systematics of oxygen isotope ratios recorded in chondrules before accretion into their parent body, *in situ* high-precision ion microprobe oxygen isotope analyses were performed for chondrules from the Acfer 094, which is an ungrouped carbonaceous chondrite (e.g., Newton et al., 1995). We analyzed oxygen isotope ratios of large minerals (>15 μm) as well as tiny minerals and glass in mesostasis (~5 μm) in individual chondrules in order to fully characterize oxygen isotope systematics. Acfer 094 is ideally suited for studying the primary oxygen isotope record of minerals and glass in chondrules because it is one of the least equilibrated carbonaceous chondrites (type 3.00, Kimura et al., 2008) and contains almost no secondary hydrous minerals (Greshake, 1997).

2. ANALYTICAL PROCEDURES

2.1. Electron microscopy and Raman spectroscopy

For petrographic observation of chondrules, backscattered electron (BSE) and secondary electron (SE) images were obtained by a Hitachi S-3400N scanning electron microscope (SEM) at University of Wisconsin-Madison (UW-Madison). Cathodoluminescence (CL) observation by SEM was also imaged for selected samples that contain CL luminous forsteritic olivine. Major element compositions in minerals and glass were obtained using the JEOL 733 electron-probe microanalyzer (EPMA) at Ibaraki University. Quantitative mineral analyses were conducted at 15 kV and a sample current of 20 nA for olivine and pyroxene, and 4 nA for glass, plagioclase, and silica. Matrix corrections were carried out by the Bence-Albee correction method.

The Raman spectra were obtained to identify silica polymorphs in chondrules using a JASCO NRS-1000 Raman microspectrometer at the National Institute of Polar Research, Japan. The laser power was 11 mW and the size of the laser beam was ~1 μm in diameter.

2.2. SIMS oxygen isotope analysis

Oxygen three-isotope analyses were performed with a Secondary Ion Mass Spectrometer (SIMS), CAMECA IMS 1280 at the WiscSIMS Laboratory, UW-Madison. The analytical conditions were similar to those of Kita et al. (2009) and Kita et al. (2010). We applied focused Cs^+ ion primary beam with 20 kV total accelerating voltage. In order to analyze individual minerals and glass without overlap, we used two different primary beam conditions: a large beam (~15 μm) with high primary ion intensity (~2.5 nA) for analysis of olivine and pyroxene phenocrysts; and a smaller beam (~3 μm) with low primary ion intensity (~25 pA) for analysis of fine-grained minerals (high-Ca pyroxene, plagioclase, silica) and glass (Fig. 1). A normal incidence electron gun and ~40 nm Au coat were used for charge compensation. Secondary ions of $^{16}O^-$, $^{17}O^-$ and $^{18}O^-$ were detected with multiple collectors simultaneously. For 15 μm spot analyses, we used three Faraday cups with a typical count rate of $^{16}O^-$ of $\sim 2 \times 10^9$ cps. For 3 μm spot analyses, we used a Faraday cup for $^{16}O^-$ and two electron multipliers for $^{17}O^-$ and $^{18}O^-$. A typical count rate of $^{16}O^-$ with a 3 μm spot was $\sim 2 \times 10^7$ cps. The mass resolving power (MRP) was set to ~2200 for $^{16}O^-$ and $^{18}O^-$. For $^{17}O^-$, we applied different settings for MRP for analyses with a 15 μm spot (MRP ~ 5000) or analyses with a 3 μm spot (MRP ~ 6000) because the relative ion intensity of $^{16}OH^-$ vs. $^{17}O^-$ is higher ($[^{16}OH^-/^{17}O^-] \sim 1$) than with a 15 μm spot analyses ($[^{16}OH^-/^{17}O^-] \sim 0.2$). The count rate of $^{16}OH^-$ was measured after each O isotope analysis and the contribution of $^{16}OH^-$ to $^{17}O^-$ was estimated assuming that both $^{16}OH^-$ and $^{17}O^-$ have the same mass spectrum (Heck et al., 2010). The estimated $^{16}OH^-$ contribution to $^{17}O^-$ was always less than $0.08‰$ for both standard and sample analyses. After the oxygen isotope analyses, all the analysis pits were observed by SEM. Data from irregular pits (e.g., pits on cracks, mixture of multiple phases) were rejected.

Measured $^{18}O/^{16}O$ and $^{17}O/^{16}O$ ratios are normalized to the VSMOW scale ($\delta^{18}O$ and $\delta^{17}O$, see McKeegan and Leshin, 2001) and the instrumental bias was corrected from analyses of a thin section of San Carlos olivine (SC-ol) standard ($\delta^{18}O = 5.32‰$; Kita et al., 2010), which was used for

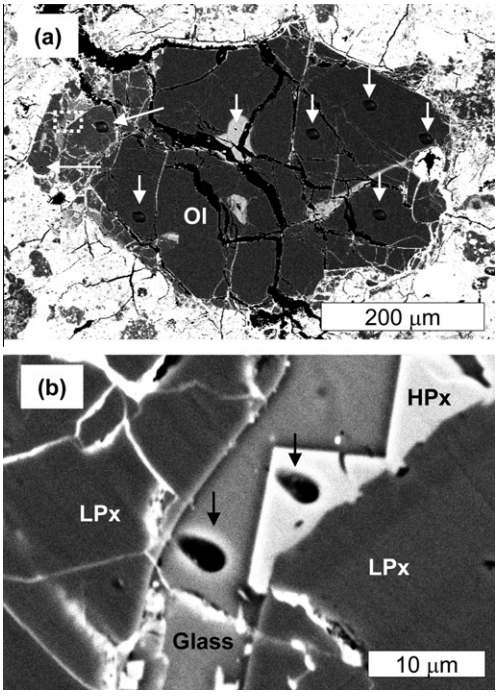

Fig. 1. Backscattered electron images of representative oxygen isotope analysis pits on G56 (type IA) with (a) ~2.5 nA, 15 μm Cs^+ beam and (b) ~25 pA, 3 μm Cs^+ beam. The dashed square in (a) indicates the field of view of (b). Analysis points are indicated by arrows. *Abbreviations*: Ol = olivine, LPx = low-Ca pyroxene, HPx = high-Ca pyroxene.

a running standard to bracket unknown chondrule analyses. Multiple mineral (low-Ca pyroxene, diopside, plagioclase, and quartz) and four geological glass standards (ML3B-G, T1-G, StHs6/80-G, ATHO-G, Jochum et al., 2006) with known oxygen isotope ratios (i.e., $\delta^{18}O$ in Vienna Standard Mean Ocean Water (VSMOW) scale) were analyzed in order to estimate the instrumental bias relative to sample matrix. The correction methods of instrumental bias are described in Kita et al. (2010). The bias correction factors of mineral and glass standards relative to SC-ol may change from session to session, depending on the primary beam conditions, and thus standards with matching matrix compositions were analyzed in the same session in order to estimate the bias correction factors more accurately. Actual bias correction factors used in this work are described in Electronic Annex EA1. The instrumental biases from sample matrix are mass dependent ($\delta^{17}O = 0.52 \times \delta^{18}O$), so that there is no measurable systematic bias in $\Delta^{17}O$ values ($=\delta^{17}O - 0.52 \times \delta^{18}O$) among different terrestrial standards (Table EA2-1 in Electronic Annex EA2).

The instrumental biases of high-Ca pyroxene, plagioclase, and glass vary linearly with molar $100 \times [CaO/(CaO + MgO + FeO)]$ (Wo), molar $100 \times [CaO/(CaO + 0.5Na_2O + 0.5K_2O)]$ (An), and SiO_2 wt.%, respectively (Fig. EA1-1 in Electronic Annex EA1). The instrumental biases of magnesian olivine and low-Ca pyroxene depend little on their molar $100 \times [MgO/(MgO + FeO)]$ (Mg#) values at Mg# ⩾ 60 (Valley and Kita, 2009), so that no correction is applied to olivine and low-Ca pyroxene based on Mg#. However, olivine and low-Ca pyroxene in the type II chondrules studied often include those with Mg# outside the range of our standards (olivine Mg# = 100–60, pyroxene Mg# = 97–70, Valley and Kita, 2009). Therefore, FeO-rich olivine (Mg# < 60) and low-Ca pyroxene (Mg# < 70) data from some chondrules would have uncertainty of the instrumental bias in $\delta^{18}O$ of up to ~1‰ at most. We applied the instrumental bias of quartz to correct that of cristobalite. Previous studies have suggested that there is not a large difference in bias among polymorphs of SiO_2 (Schulze et al., 2003), but this has not been evaluated yet for cristobalite. The $\Delta^{17}O$ values of such samples are not affected.

The analytical uncertainty of individual analyses of unknowns is calculated based on the spot-to-spot reproducibility (±2SD, standard deviation) of the eight bracketing SC-ol standard analyses (Kita et al., 2009; Valley and Kita, 2009). Typical 2SD errors of $\delta^{18}O$, $\delta^{17}O$, and $\Delta^{17}O$ with the high intensity beam are ±0.3, ±0.6, and ±0.6‰, respectively. Those of $\delta^{18}O$, $\delta^{17}O$, and $\Delta^{17}O$ with the low intensity beam are ±1.2, ±1.2, and ±1.1‰, respectively.

3. SAMPLE SELECTION

We chose 57 chondrules including nine large olivine fragments (possibly chondrule fragments) from a thin section of Acfer 094 chondrite (USNM 7233-6) based on size of the chondrule (typically >200 μm in diameter) and petrologic characteristics (e.g., type I vs. type II, silica-bearing chondrules, plagioclase-rich chondrule). After EPMA analysis, we selected 42 chondrules for oxygen isotope analysis based on the position in the thin section and petrologic type of the chondrules as described below.

The selected samples include 29 type I (FeO-poor, Mg# ⩾ 90) chondrules (Fig. 2a–c), 12 type II (FeO-rich, Mg# < 90) chondrules (Fig. 2d), and one Al-rich chondrule (Fig. 2e). Six out of 29 type I chondrules are classified as refractory forsterite (RF) bearing chondrules (RF-type I in the Table 1 and Fig. 2c) because they contain forsterite grains with >0.5 wt.% CaO (Steele, 1986). CL images of RF-type I chondrules are shown in Fig. EA3 in Electronic Annex EA3. CL images are useful to recognize highly magnesian refractory forsterite that shows luminous blue CL. In addition to typical porphyritic olivine and/or pyroxene chondrules, the samples include non-porphyritic chondrules that have been totally melted and rapidly cooled such as two radial pyroxene (RP) chondrules (1 type I and 1 type II), one barred olivine (BO) chondrule (type I: Fig. 2f), one cryptocrystalline (CC) chondrule (type I: Fig. 2g), two silica-bearing chondrules (1 type I and 1 type II: Fig. 2h). The silica minerals in two silica-bearing chondrules show strong peaks at 419.4 and 228.4 cm^{-1}, characteristic of cristobalite (Kimura et al., 2005). Existence of cristobalite in these chondrules indicates that they formed by rapid cooling from melt after crystallization (Hezel et al., 2003). Three large olivine fragments (possibly porphyritic chondrule fragments: 1 type I, 1 RF-bearing type I, and 1 type II) were also analyzed. The sample names and petrologic features of chondrules are summarized in Table 1. Backscattered electron images of chondrules that

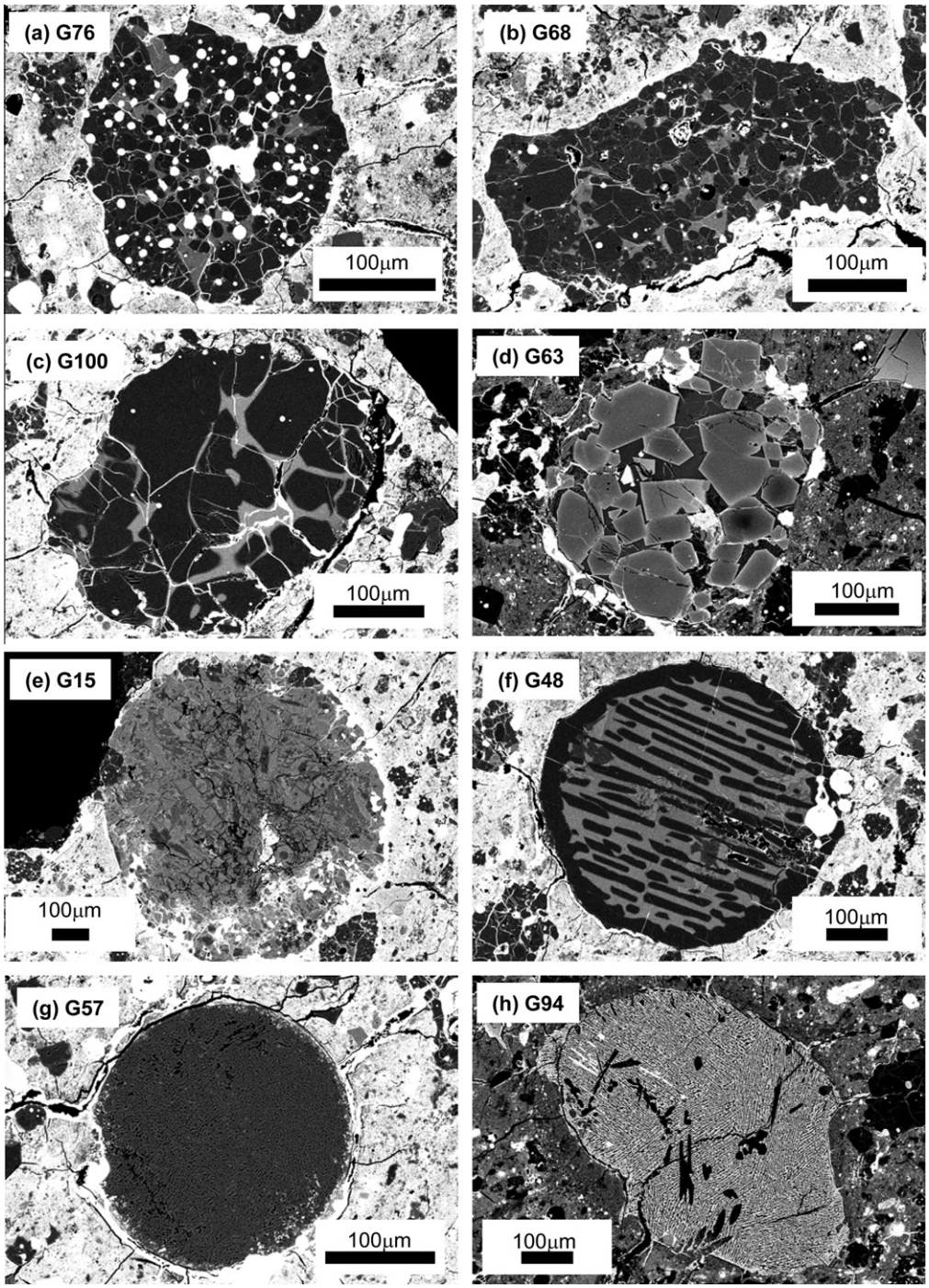

Fig. 2. Backscattered electron (BSE) images of typical chondrules from Acfer 094. (a) type IAB chondrule G76, (b) type IAB chondrule G68, (c) Refractory forsterite (RF) bearing type IA chondrule G100, (d) type II chondrule G63, (e) Al-rich chondrule G15, (f) type I barred olivine chondrule G48, (g) type IB cryptocrystalline chondrule G57, and (h) Silica-bearing type II chondrule G94. Brightness and contrast of the BSE images for type II chondrules are individually adjusted to show texture clearly. Oxygen isotope analysis points and minerals are shown in Fig. EA3 in the Appendix.

we analyzed for oxygen isotopes in this study are shown in Electronic Annex EA3.

During the selection of chondrules for oxygen isotope analysis, we intentionally selected more from the less-abundant groups of chondrules than the major type I porphyritic olivine-pyroxene chondrules with the purpose of understanding the oxygen isotope systematics among various types of chondrules. As a result, selected chondrules for isotope analysis are slightly biased towards more type II and RF-bearing type I chondrules. We selected 12 type II chondrules out of 42 chondrules, which is higher than the frequency of type II chondrules in Acfer 094 (~20%,

Table 1
Petrologic type, elemental compositions of olivine and pyroxene phenocrysts, and averaged oxygen isotope ratios of host chondrules.

Sample name	Type[2]	Texture	Mg#[4]	Olivine	Low-Ca pyroxene	High-Ca pyroxene[6]	Feldspar[6]	Glass[6]	Averaged oxygen isotope ratios			Relict olivine[6]	Distance from center[7]
				Fo[5]	En[5]				$\delta^{18}O$	$\delta^{17}O$	$\Delta^{17}O$		
Acfer 094 (USNM 7233-8)													
Al-rich													
G15	Al-rich	Porphyritic	99.1		91.3 (85.4–97.8)	+	+	+	-3.74 ± 0.85	-6.59 ± 0.44	-4.64 ± 0.42		<5.0 mm
RF-type I													
G100	RF-IA	Porphyritic	99.5	99.5 (99.1–99.7)				+	Heterogeneous			+	5.3 mm
G13	RF-IAB	Porphyritic	98.8	99.2 (98.9–99.5)	92.5 (84.2–97.7)	+	+	+	Heterogeneous			+	<5.0 mm
G56	RF-IAB	Porphyritic	99.5	99.4 (99.2–99.6)	98.2 (97.6–98.7)	+		+	-5.86 ± 0.32	-8.60 ± 0.39	-5.55 ± 0.37		<5.0 mm
G67	RF-IAB	Porphyritic	99.2	99.4 (99.0–99.6)	97.2 (95.0–98.2)			+	-6.72 ± 0.33	-9.62 ± 0.42	-6.12 ± 0.39		<5.0 mm
G77	RF-IAB	Porphyritic	99.3	99.3 (99.1–99.5)		+		+	-4.71 ± 0.40	-7.43 ± 0.32	-4.98 ± 0.19		5.2 mm
G113	RF-I	Olivine fragment	99.5	99.5 (99.0–99.6)					-6.82 ± 0.33	-9.82 ± 0.29	-6.27 ± 0.27		<5.0 mm
Type I (Mg# > *98)*													
G7	IAB	Porphyritic	98.5	98.8 (98.5–98.9)	97.7 (97.4–97.9)	+	+	+	-3.39 ± 0.49	-6.82 ± 0.48	-5.06 ± 0.38	+	<5.0 mm
G18[1]	IAB	Porphyritic	98.3	98.6 (98.5–98.6)	96.6 (93.6–97.7)	+	+	+	-6.51 ± 0.92	-8.71 ± 0.67	-5.33 ± 0.65		<5.0 mm
G26	IAB	Porphyritic	98.9	98.9 (98.8–99.2)	98.0 (97.6–98.3)	+		+	-5.53 ± 0.31	-7.87 ± 0.50	-4.99 ± 0.46	+	<5.0 mm
G38	IAB	Porphyritic	99.1	99.1 (99.0–99.2)	95.9 (94.3–97.7)	+		+	-3.73 ± 0.74	-6.73 ± 0.62	-4.79 ± 0.31		<5.0 mm
G42[1]	IAB	Porphyritic	98.4	98.8 (98.4–99.1)	96.0 (95.0–97.6)	+	+		-6.30 ± 0.95	-8.61 ± 0.68	-5.47 ± 0.47		<5.0 mm
G46	IAB	Porphyritic	98.9	98.8 (98.6–99.0)	97.9 (97.6–98.2)	+	+		-4.59 ± 0.53	-7.27 ± 0.39	-4.88 ± 0.29	+	<5.0 mm
G68	IAB	Porphyritic	98.0	98.7 (98.5–98.8)	93.4 (86.6–97.7)	+	+		Heterogeneous			+	<5.0 mm
G70	IAB	Porphyritic	99.0	99.1 (98.9–99.3)	97.8 (97.8–97.8)	+		+	-6.54 ± 0.44	-9.11 ± 0.27	-5.70 ± 0.22	+	<5.0 mm
G73	IAB	Porphyritic	99.1	99.2 (99.1–99.4)	97.4 (97.1–97.7)		+		-6.80 ± 0.81	-9.70 ± 0.54	-6.16 ± 0.24		5.6 mm
G76[1]	IAB	Porphyritic	98.5	98.4 (98.2–98.7)	97.7 (97.5–97.8)	+	+		-3.47 ± 0.40	-6.88 ± 0.84	-5.08 ± 0.78		5.6 mm
G81	IAB	Porphyritic	99.1	99.1 (99.0–99.2)	98.1 (98.0–98.2)	+	+	+	-5.80 ± 0.41	-8.90 ± 0.43	-5.89 ± 0.42	+	<5.0 mm
G84	IAB	Porphyritic	99.0	99.2 (99.0–99.4)	98.0 (98.0–98.0)			+	Heterogeneous			+	<5.0 mm
G87[1]	IAB	Porphyritic	99.1	99.2 (98.9–99.4)	97.5 (96.0–98.1)	+	+		-12.73 ± 0.54	-15.95 ± 0.68	-9.33 ± 0.60		<5.0 mm
G95	IAB	Porphyritic	98.7	98.7 (98.6–98.7)	97.8 (96.6–98.2)		+		-3.41 ± 0.37	-6.54 ± 0.26	-4.77 ± 0.26		6.1 mm
G64[1]	IB	Porphyritic, dusty olivine	99.0	98.6 (97.7–99.3)	98.2 (97.9–98.4)	+		+	1.48 ± 1.01	-1.06 ± 0.83	-1.83 ± 0.66	+	<5.0 mm
G48[1]	I	Barred ol	99.4	99.4 (99.2–99.4)	93.1 (89.8–94.9)	+		+	-3.78 ± 0.72	-7.25 ± 0.68	-5.28 ± 0.49		<5.0 mm
G90[1]	I	Silica-bearing[3]	99.2	99.2 (99.1–99.4)	85.3 (85.3–85.3)	+		+	-6.86 ± 1.12	-10.47 ± 0.95	-6.91 ± 0.79		5.9 mm
Type I (90 < Mg# < *98)*													
G52	IA	Porphyritic	94.6	94.6 (94.3–94.9)				+	1.88 ± 0.36	-1.22 ± 0.52	-2.19 ± 0.51	+	<5.0 mm
G45	IAB	Porphyritic	95.2	95.6 (95.4–95.8)	92.5 (89.1–95.6)		+		0.66 ± 0.39	-2.08 ± 0.38	-2.42 ± 0.36	+	<5.0 mm
G74	IAB	Porphyritic	94.5	94.6 (93.3–95.4)	91.2 (91.2–91.2)	+	+		1.50 ± 0.61	-1.15 ± 0.44	-1.93 ± 0.25	+	6.0 mm
G27	I	Radial pyroxene	91.4		88.2 (86.2–89.1)				0.40 ± 0.36	-1.89 ± 0.25	-2.10 ± 0.22		<5.0 mm
G39	I	Olivine fragment	92.3	92.3 (88.8–96.0)		+	+		3.12 ± 0.51	1.12 ± 0.39	-0.51 ± 0.37		<5.0 mm
G57	I	Cryptocrystalline	96.0						-5.35 ± 0.63	-7.70 ± 0.47	-4.91 ± 0.44		<5.0 mm

(*continued on next page*)

Table 1 (*continued*)

Sample name	Type[2]	Texture	Mg#[4]	Olivine Fo[5]	Low-Ca pyroxene En[5]	High-Ca pyroxene[6]	Feldspar[6]	Glass[6]	Averaged oxygen isotope ratios $\delta^{18}O$	$\delta^{17}O$	$\Delta^{17}O$	Relict olivine[6]	Distance from center[7]
Type II (Mg# < *90*)													
G6	IIA	Porphyritic	49.7	49.7 (38.9–63.1)				+	1.57 ± 0.50	−1.51 ± 0.50	−2.27 ± 0.19		<5.0 mm
G10	IIA	Porphyritic	67.8	67.8 (53.3–95.9)		+		+	−0.03 ± 1.20	−2.79 ± 1.05	−2.78 ± 0.53	+	<5.0 mm
G34	IIA	Porphyritic	77.1	77.1 (66.6–96.2)				+	1.79 ± 0.71	−1.83 ± 0.52	−2.75 ± 0.53	+	<5.0 mm
G63	IIA	Porphyritic	62.1	62.1 (52.7–86.2)				+	0.72 ± 0.39	−2.01 ± 0.64	−2.54 ± 0.50	+	<5.0 mm
G71	IIA	Porphyritic	67.6	67.6 (54.2–96.3)				+	2.07 ± 0.49	−0.98 ± 0.45	−2.05 ± 0.27	+	5.1 mm
G75[1]	IIA	Porphyritic	75.4	75.4 (59.5–93.8)		+	+	+	2.39 ± 1.96	−0.42 ± 1.68	−1.72 ± 0.66	+	<5.0 mm
G86	IIA	Porphyritic	60.0	60.0 (47.2–70.7)		+	+		1.63 ± 0.36	−1.49 ± 0.73	−2.34 ± 0.61	+	<5.0 mm
G79	IIAB	Porphyritic	42.2	36.5 (14.9–48.5)	44.7 (34.0–53.8)			+	–[8]	–[8]	−1.54 ± 0.32		<5.0 mm
G85	IIB	Porphyritic	87.1		86.0 (82.6–88.9)	+	+	+	2.70 ± 0.39	1.46 ± 0.22	0.06 ± 0.25		<5.0 mm
G32	II	Olivine fragment	60.1	60.1 (51.5–76.2)				+	2.26 ± 0.36	−1.41 ± 0.31	−2.54 ± 0.29		7.8 mm
G35[1]	IIAB	Radial pyroxene	46.1	35.4 (34.4–37.1)	49.0 (44.4–55.0)			+	–[8]	–[8]	−2.07 ± 0.80		<5.0 mm
G94[1]	II	Silica-bearing[3]	41.6	38.3 (37.9–38.5)	42.2 (41.7–42.8)				–[8]	–[8]	−1.82 ± 0.56		6.6 mm

[1] The average values were based on data of 3 μm beam analyses.
[2] RF = refractory forsterite bearing, I = type I, II = type II, A = predominately olivine phenocrysts, AB = olivine and pyroxene phenocrysts.
[3] Cristobalite identifed by Raman spectroscopy.
[4] Averaged number of olivine and low-Ca pyroxene.
[5] Average composition and range (in parenthesis).
[6] + indicates occurrence in the chondrule.
[7] Sample position from the center of the ion microprobe holder.
[8] The average value is not calculated because of no appropriate standards.

Kunihiro et al., 2005). From a total of 41 type I chondrules that were examined by EPMA and CL images, we selected all of the RF-bearing type I chondrules (total 6), but only 23 non-RF bearing type I chondrules. Nonetheless, our selected chondrules generally cover the representative chondrule types in the meteorite.

Position of chondrules near the center of a 25 mm diameter thin section was also a criterion for sample selection. The section is mounted in a sample holder that has a 100 μm thick tungsten lip with 20 mm diameter window, to which −10 kV extraction voltage is applied. Analysis of chondrules located near the lip would show additional instrumental bias due to the deformation of the ion extraction field. Kita et al. (2009) demonstrated that variation of the analytical bias due to stage position (measured $\delta^{18}O$ value) is comparable to the reproducibility of the repeated analyses at the center of the sample holder (~±0.3‰, 2SD) if the analysis point is within 6 to 7 mm from the center of the sample holder. Most chondrules analyzed in this work were chosen within 5 mm from the center of the sample holder. Distances of chondrules from the center of the sample holder are shown in Table 1 if they are more than 5 mm. Two samples among the selected chondrules were located significantly farther from the center, 7.8 mm and 6.6 mm for FeO-rich olivine fragment G32 and FeO-rich silica-bearing chondrule G94, respectively. These samples were chosen due to their uncommon mineralogy and chemistry even though data could be slightly biased. The effect of sample stage position on oxygen three-isotope ratios is likely mass dependent, so that $\Delta^{17}O$ values would not be affected.

4. RESULTS

The major element compositions of individual minerals in chondrules were obtained using EPMA (more than 20 analyses per chondrule) and summarized in Table 1. Representative major element analyses of minerals in various types of chondrules are shown in Table EA2-2 in Electronic Annex EA2. We performed 340 oxygen isotope analyses (191 with a 15 μm spot and 149 with a 3 μm spot) from 42 chondrules from Acfer 094 chondrite. Oxygen three-isotope plots of individual chondrules are shown in Figs. 4–8. The oxygen isotope data of individual chondrules are summarized in Table EA2-3 and analysis points are shown in Fig. EA3. The EPMA analyses of high-Ca pyroxene, plagioclase and glass from the same locations as the SIMS analyses (summarized in Table EA2-3) were used to calculate instrumental bias due to sample matrix as a function of Wo mol%, An mol%, and SiO_2 wt.%, respectively, as described in EA1. The full data sets including analyses of running standards for these two analysis sessions are shown in Tables EA2-4 and EA2-5. A number of oxygen isotope analyses for each chondrule sample (2–14 points each) were made according to texture, mineralogy, and observed oxygen isotopic heterogeneity of the sample.

4.1. $\Delta^{17}O$ Values in individual chondrules

Many chondrules from Acfer 094 show internal oxygen isotope heterogeneity beyond analytical uncertainties. Examples of chondrules with internally heterogeneous oxygen isotope ratios are shown in Fig. 3. Oxygen isotope ratios of individual minerals in these chondrules are distributed along a slope ~1 line in an oxygen three-isotope diagram (Fig. 3e–h). In most cases, while a majority of data in a single chondrule show either indistinguishable or a relatively narrow range of oxygen isotope ratios (⩽few ‰), distinctively different oxygen isotope ratios are observed among a few analyses or less, exclusively from olivine (Fig. 3e–g). In a few cases, oxygen isotope ratios in a chondrule are entirely heterogeneous, spanning over 40‰ (Fig. 3h). To distinguish heterogeneity of oxygen ratios in individual chondrules, we calculated $\Delta^{17}O$, which represents deviation of oxygen isotope ratios from the terrestrial mass fractionation line (TF line; $\Delta^{17}O \equiv 0$). Because mass dependent fractionation of $\delta^{18}O$ vs. $\delta^{17}O$ along slopes parallel to the TF line may occur during chondrule formation by chemical and/or physical processes even from an initially homogeneous oxygen isotope reservoir, $\Delta^{17}O$ is a convenient notation to describe oxygen isotope heterogeneity. Analyses with a 15 μm spot have significantly better precision than smaller spots and are most commonly used in the examination of internal heterogeneity. Distribution of $\Delta^{17}O$ values in chondrules changes systematically with chondrule types (i.e., texture and mineral chemistry), as summarized below.

4.1.1. Non-porphyritic chondrules and an Al-rich chondrule

We measured oxygen isotope ratios of six non-porphyritic chondrules with textures that indicate crystallization after the total melting and rapid cooling. They include one barred olivine (BO) chondrule (G48, Fig. 2f), two radial pyroxene (RP) chondrules (G27 and G35), one cryptocrystalline (CC) chondrule (G57, Fig. 2g), and two silica-bearing chondrules (G90 and G94, Fig. 2h). Oxygen isotope ratios of multiple phases in an individual chondrule are generally homogeneous and consistent with high temperature equilibration (Fig. 4). Although oxygen isotope ratios for cristobalite in G90 (Fig. 4c) and G94 (Fig. 4g) plot to the right of other minerals, this could be a result of an analytical artifact due to lack of a cristobalite standard. The $\Delta^{17}O$ values of multiple analyses in each chondrule are identical within the external reproducibility (Table EA2-3).

We also measured oxygen isotope ratios of minerals in an Al-rich chondrule (G15), which mostly consists of low-Ca pyroxene, high-Ca pyroxene, and plagioclase (Figs. 2e and 4a). No resolvable difference in $\Delta^{17}O$ values are observed among these analyses.

4.1.2. Type II porphyritic chondrules

Oxygen isotope ratios of individual porphyritic type II chondrules are shown in Figs. 3e and 5. Most type II porphyritic chondrules are distributed at $\delta^{18}O > 0$‰ and some olivine grains' data are distributed along a slope of ~1 line. Internal variations in $\Delta^{17}O$ are observed in 6 out of 10 type II porphyritic chondrules (Table EA2-3). In most cases, relatively lower $\Delta^{17}O$ values (−5 to −7‰) are observed in forsteritic cores (Mg# = 96–86) of strongly zoned olivine phenocrysts, in contrast to higher $\Delta^{17}O$ values (−2 to −3‰) at the fayalitic rim (Mg#~60, e.g., Fig. 3a, e and i).

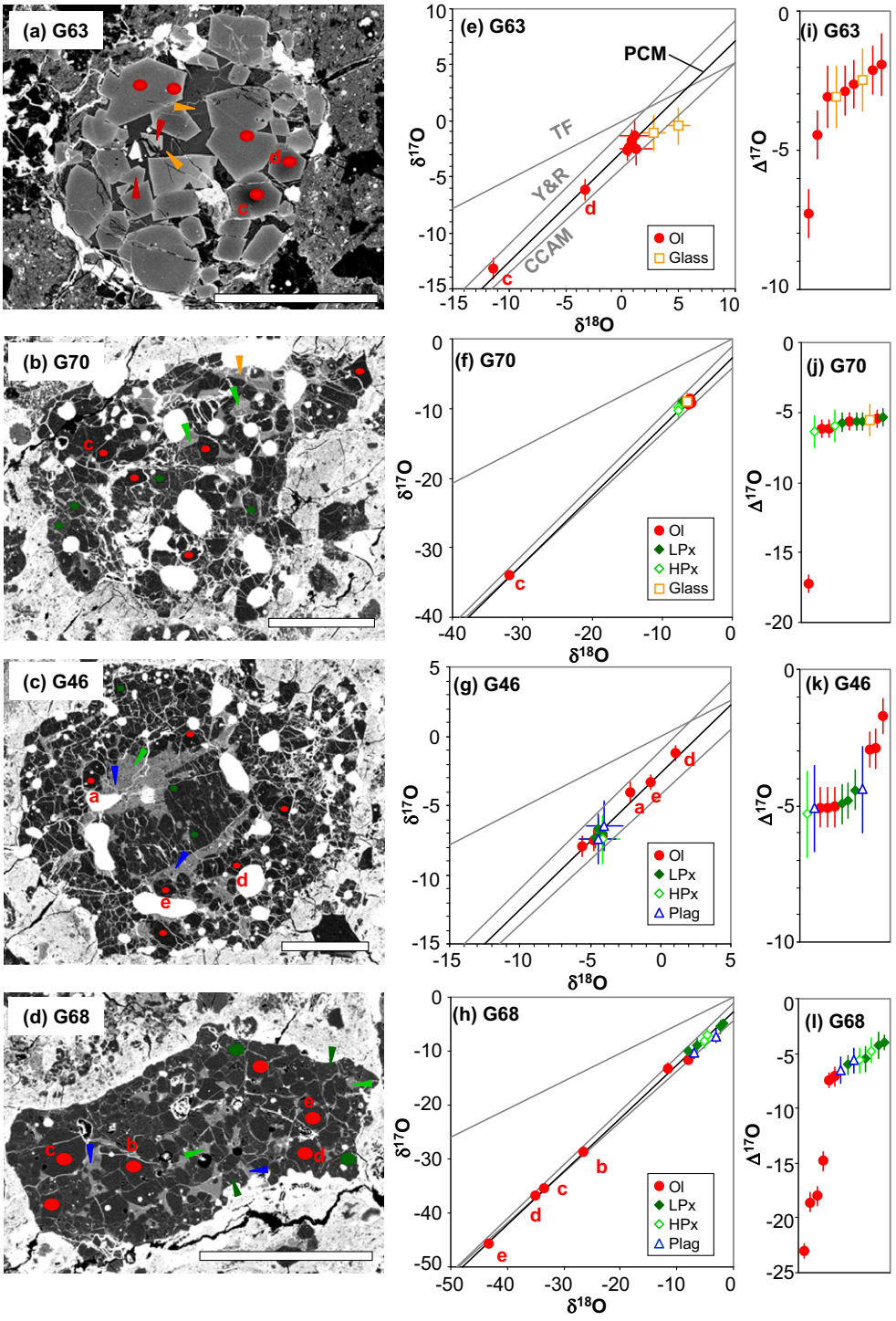

Fig. 3. Backscattered electron images with oxygen isotope analysis points, oxygen three-isotope plots, and $\Delta^{17}O$ value plots of representative chondrules from Acfer 094. (a–d) Backscattered electron images of G63 (type IIA), G70 (type IAB), G46 (type IAB), and G68 (type IAB), respectively. Analysis points are shown by an ellipse for ~15 μm beam spots and the vertex of a triangle for ~3 μm beam. Colors of symbols are the same as those of oxygen-three isotope plots. Scale bar indicates 200μm. (e–h) Oxygen three-isotope plots of data from G63, G70, G46, and G68, respectively. Three gray lines, CCAM, Y&R, and TF, represent Carbonaceous Chondrite Anhydrous Minerals line, Young and Russell line, and Terrestrial Fractionation line, respectively. The black PCM line represents the correlation line from oxygen isotope data in this study (see Section 5.4). Error bars are 2SD. (i–l) The $\Delta^{17}O$ values of data from G63, G70, G46, and G68, respectively. Data are shown in ascending sequence. Symbols are the same as oxygen three-isotope plots. Error bars are 2SD.

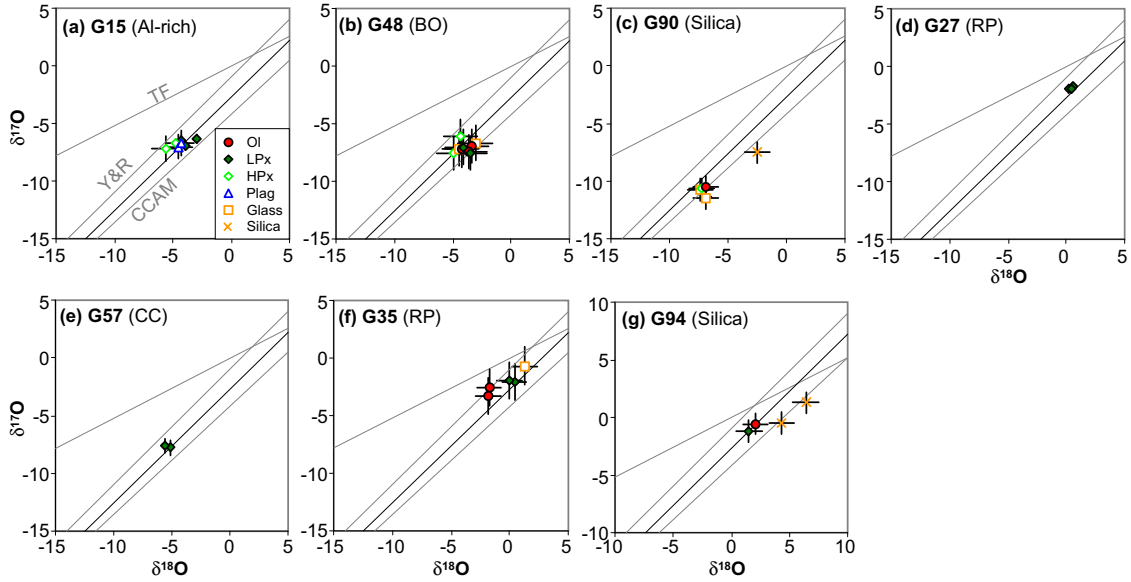

Fig. 4. Oxygen three-isotope plots of an Al-rich chondrule and non-porphyritic chondrules. The order of plots of chondrules is same as that of Table 1. Four reference lines are the same as Fig. 3. Error bars are 2SD.

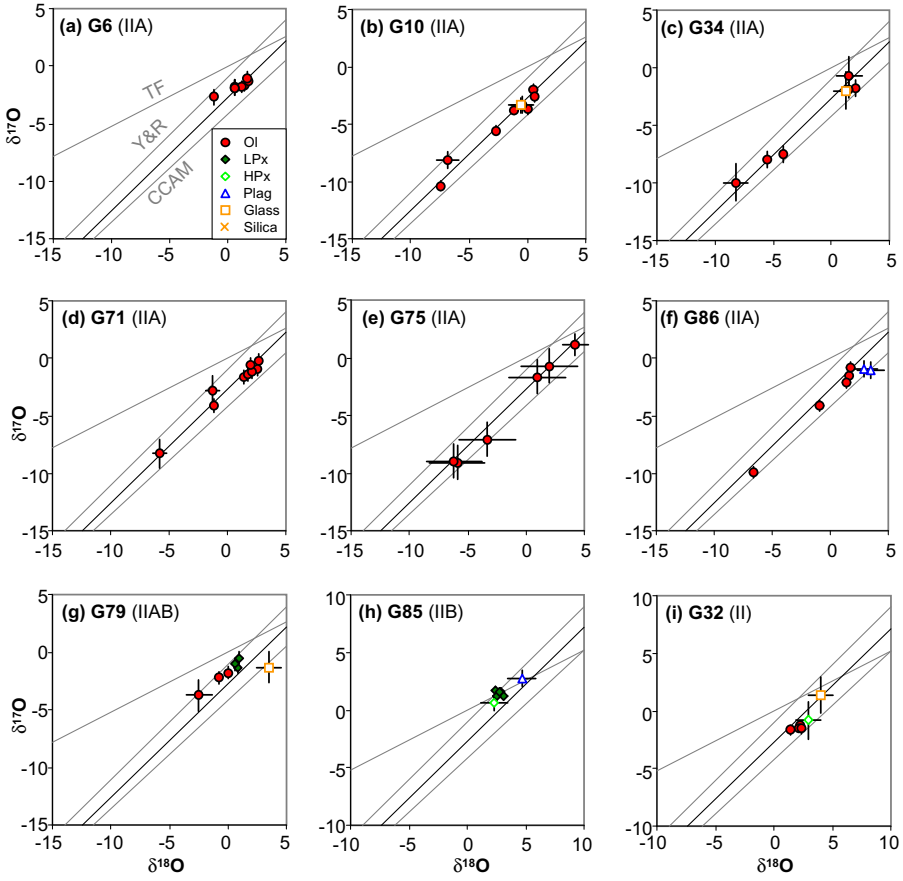

Fig. 5. Oxygen three-isotope plots of type II porphyritic chondrules excluding G63, which is shown in Fig. 3. The order of plots of chondrules is same as that of Table 1. Four reference lines are the same as Fig. 3. Error bars are 2SD.

Similar oxygen isotope anomalies in forsteritic olivine cores in type II chondrules have been reported previously (e.g., Yurimoto and Wasson, 2002; Kunihiro et al., 2004, 2005). This is consistent with the idea that the forsteritic core of olivine phenocrysts in type II chondrules is an unmelted "relict" olivine grain from a solid precursor of the chondrule and their oxygen isotope ratios never equilibrated with the final chondrule-forming melt (e.g., Nagahara, 1981) although such exchange is possible (Boesenberg et al., 2004, 2008). In contrast, the fayalitic rims of olivine phenocrysts, pyroxene, and glass show relatively higher $\Delta^{17}O$ values at −2 to −3‰ and are indistinguishable within individual chondrules (e.g., G63, Fig. 3a, e and i). In some cases, ferroan olivine grains that are not recognized as relict olivine grains from chemical compositions have distinct oxygen isotope ratios compared to other analyses in the same chondrule (G34, G75, and G86, Table 1 and Table AE2-3). Two pyroxene-rich type II porphyritic chondrules (G79 and G85) are internally homogeneous in $\Delta^{17}O$ although oxygen isotope ratios of mesostasis are positively fractionated beyond the analytical uncertainty (Fig. 5g and h).

4.1.3. Type I porphyritic chondrules

Oxygen isotope data of individual type I and RF-bearing type I porphyritic chondrules are shown in Fig. 6 (for Mg# = 90–98), Fig. 7 (for Mg# > 98), and Fig. 8 (for RF-bearing type I). Oxygen isotope ratios of relatively FeO-rich (Mg# = 90–98) type I chondrules tend to be distributed at $\delta^{18}O > 0‰$ (Fig. 6). In contrast, those of type I with Mg# > 98 and RF-bearing type I chondrules are mostly distributed at $\delta^{18}O < 0‰$ (Figs. 7 and 8). Internal variations in $\Delta^{17}O$ are also observed in type I porphyritic chondrules (3 out of 4 for Mg# = 90–98 and 8 out of 15 for Mg# > 98, respectively) and RF-bearing type I (2 out of 6). In these chondrules, some olivine grains show variable $\Delta^{17}O$ values while other olivine and low-Ca pyroxene grains, and high Ca-pyroxene and plagioclase in the mesostasis in the same chondrule show consistent $\Delta^{17}O$ values (Fig. 3j and k). In a few chondrules (G68 and G84), most data show variable $\Delta^{17}O$ values beyond the analytical uncertainty, some of which approach values as low as −23‰ (Figs. 3l and 7i) similar to those observed in CAIs (e.g., Yurimoto et al., 2008). Olivine grains with distinct $\Delta^{17}O$ values from others in the same chondrule are thus interpreted to be "relict olivines" that survived the last melting of chondrules, even though their mineral compositions are not distinguishable from other olivine grains in the chondrule, unlike forsteritic olivine in type II chondrules. Dusty olivine grains in G64 are an exception. Many of these relict olivine grains are ^{16}O-rich compared to other analyses in the same chondrules (Fig. 3f and h), similar to the case reported in the literature (Yurimoto and Wasson, 2002; Jones et al., 2004; Kunihiro et al., 2004, 2005; Ruzicka et al., 2007; Kita et al., 2010). In the Acfer 094 chondrules, we also found several type I chondrules having ^{16}O-poor relict olivine grains that differ in $\Delta^{17}O$ by 1–3‰ compared to the $\Delta^{17}O$ values of other minerals (e.g., G46, Fig. 3k). In G26, G46, and G81, $\Delta^{17}O$ values of relict olivine grains are up to −3.5‰, −2‰, and −4‰, respectively, which are resolved from those of the rest of data in the same chondrules (−6 to −5‰, Figs. 3k and 7c,h, Table EA2-3). In G64, $\Delta^{17}O$ values of olivine grains including a dusty olivine grain are ~0‰, while all those of pyroxene and glass are ~−2‰ (Fig. 7l, Table EA2-3). Only a few similar cases with ^{16}O-poor relict olivine grains were previously reported (Kunihiro et al., 2004, 2005; Kita et al., 2010). Interestingly, all the heterogeneous chondrules examined in this study contain relict olivine grains that are either ^{16}O-poor or ^{16}O-rich, but not both, relative to other minerals in the same chondrule.

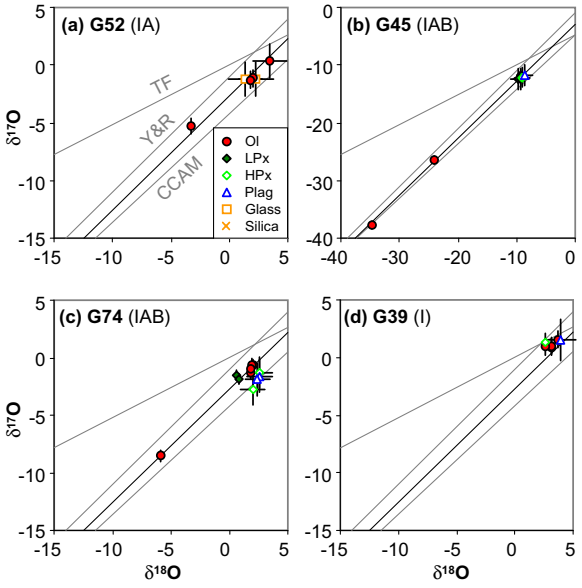

Fig. 6. Oxygen three-isotope plots of type I porphyritic chondrules with Mg# = 90–98. The order of plots of chondrules is same as that of Table 1. Four reference lines are the same as Fig. 3. Error bars are 2SD.

Two RF-bearing type I chondrules (G13 and G100) show variable oxygen isotope ratios, though the ranges of variation of $\Delta^{17}O$ values are relatively small (~1‰ in G13 and ~4‰ in G100, Fig. 8a and b, Table EA2-3). In both chondrules, olivine grains near the center of chondrules show the lowest $\Delta^{17}O$ values. In G13, $\Delta^{17}O$ values of pyroxene (from −4 to −5‰) are not well resolved from those of olivine. In G100, $\Delta^{17}O$ values of glass are similar to that of olivine grains near the edge of the chondrule (~−2.5‰, Table EA2-3, Fig. EA3).

4.2. Characteristic oxygen isotope ratios of individual chondrules

Results of oxygen three-isotope analyses of individual chondrules indicate that most chondrules consist largely of phenocrysts and mesostasis having identical $\Delta^{17}O$ values within analytical uncertainties. Here, we estimate the average oxygen three-isotope ratios of individual chondrules by excluding the contribution of relict olivine grains.

4.2.1. Methods

As noted earlier, recognition of relict olivine grains by oxygen isotope anomaly depends on the scale of isotope

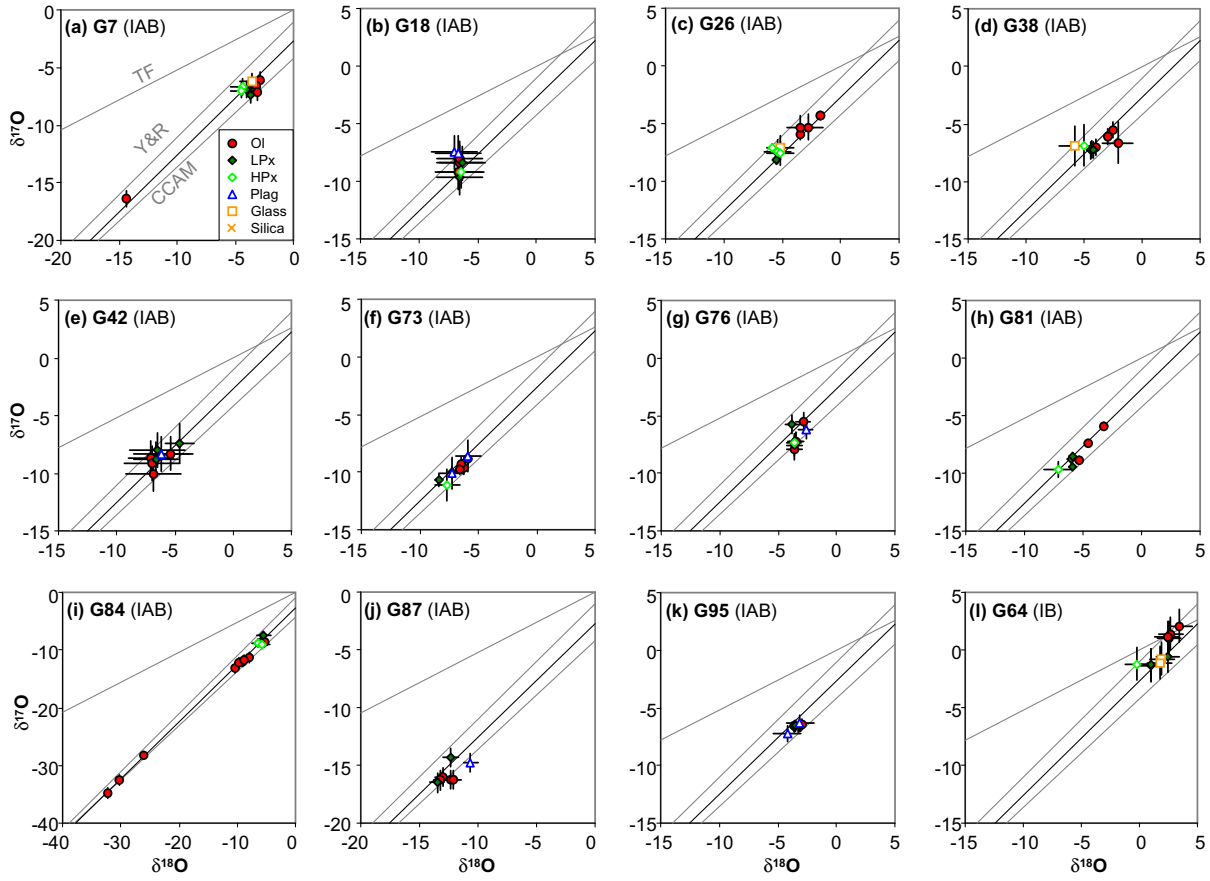

Fig. 7. Oxygen three-isotope plots of type I porphyritic chondrules with Mg# > 98 excluding G46, G68, and G70, which are shown in Fig. 3. The order of plots of chondrules is same as that of Table 1. Four reference lines are the same as Fig. 3. Error bars are 2SD.

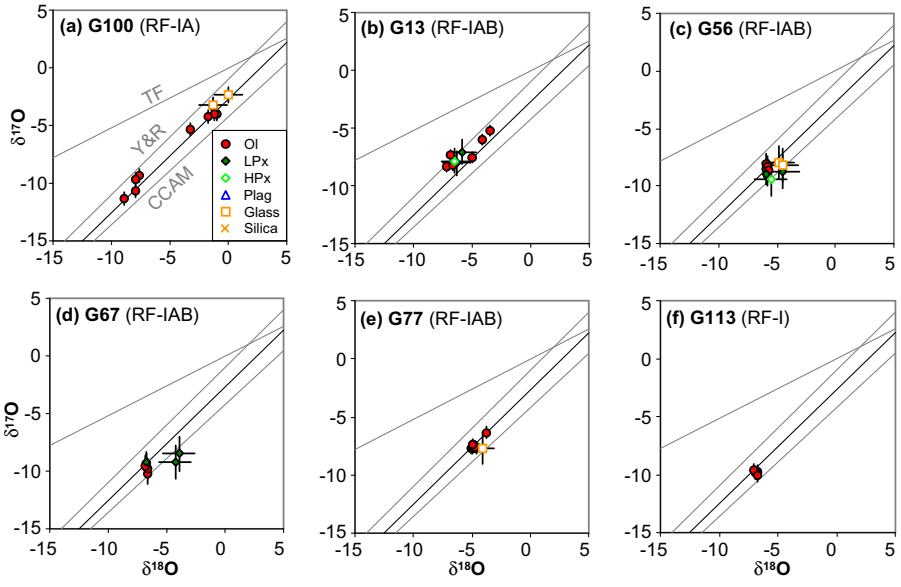

Fig. 8. Oxygen three-isotope plots of RF-bearing type I chondrules. The order of plots of chondrules is same as that of Table 1. Four reference lines are the same as Fig. 3. Error bars are 2SD.

heterogeneity compared to the analytical precisions. Our data combine two analysis sessions with different beam sizes and analytical uncertainty in $\Delta^{17}O$ measurements (i.e., typically ±0.6‰ for 15 μm beam analyses and ±1.1‰ for 3 μm beam analyses) and the number of analyses vary depending on the size of phenocrysts. We calculate the average oxygen isotope ratios of individual chondrules based on following procedures:

(1) When we could obtain oxygen isotope data with a higher-precision 15 μm beam, we calculated average oxygen isotope ratios of individual chondrules using oxygen isotope data of olivine and low-Ca pyroxene phenocrysts whose $\Delta^{17}O$ values cluster within 3SD of analytical uncertainty. We did not use oxygen isotope data of high-Ca pyroxene, plagioclase, silica, and glass in mesostasis because most data were obtained by using low precision 3 μm beam analyses.
(2) Ten chondrules were analyzed only at lower-precision 3 μm beam conditions. The average oxygen isotope ratios are calculated using 3 μm beam analyses for these chondrules. To be consistent with the calculation for other chondrules with 15 μm beam analyses, the average values are calculated using data from olivine and low-Ca pyroxene phenocrysts that are indistinguishable in $\Delta^{17}O$ values within 3SD of analytical uncertainty.
(3) Because of the lack of standards for low Mg# olivine and low-Ca pyroxene, we did not use measured $\delta^{18}O$ and $\delta^{17}O$ values of olivine with Mg# < 60 and low-Ca pyroxene with Mg# < 70 to calculate the average oxygen isotope ratios. We used the measured $\Delta^{17}O$ values of low Mg# olivine and low-Ca pyroxene because the matrix effect of the instrumental bias of the ion microprobe is mass-dependent and it does not affect to the measured $\Delta^{17}O$ values.
(4) Uncertainties of the average values are estimated at 95% confidence levels. Errors of average $\Delta^{17}O$ values are either the 2SE (twice the standard error of the mean) of data or 2σ of the weighted mean based on the uncertainty of individual data, whichever is largest. Errors of average $\delta^{18}O$ and $\delta^{17}O$ values are either the 2SE of data or the uncertainty of single analyses (as determined by 2SD of 8 bracketing standard analyses) divided by square root of the number of data (n), whichever is largest. Additional uncertainties from instrumental bias corrections, ±0.3‰ and ±0.15‰ for $\delta^{18}O$ and $\delta^{17}O$ measurements, respectively are added, so that they are propagated to the final error estimates, as described by Kita et al. (2010).

The average oxygen isotope ratios of individual chondrules are listed in Table 1. Selections of data that were used to calculate individual average values are shown in Table EA2-3. For four chondrules (G13, G68, G84, and G100), the entire chondrule data set is scattered without clustering of data within 3SD limits (Figs. 3h, 7i and 8a,b). We did not obtain the average oxygen isotope ratios for these chondrules, which are noted as "heterogeneous" in Table 1. For type II chondrules G35 and G94, the average $\delta^{18}O$ and $\delta^{17}O$ values are not calculated, but only the average $\Delta^{17}O$ values are shown, because all data were derived from olivine and pyroxene with Mg# < 60 in these chondrules. In the above calculations, relict grains whose $\Delta^{17}O$ values differ by more than 2‰ and 3‰ from the rest of analyses in the same chondrules are eliminated from the average for data using 15 μm beam and 3 μm beam condition, respectively. There are four chondrules with 8 data points (out of total 340 analyses) that were at the margin of the 3SD limit and treated differently from the above descriptions for including or not including in the average values. Detailed explanations are found in Electronic Annex EA1.

4.2.2. Phenocrysts, glass, and "host chondrule"

The $\Delta^{17}O$ values of high-Ca pyroxene, plagioclase, silica, and glass in mesostasis (Table EA2-3) are consistent with the average $\Delta^{17}O$ values of chondrules listed in Table 1 (olivine and low-Ca pyroxene phenocrysts) within the analytical uncertainty. In Fig. 9, the $\Delta^{17}O$ and $\delta^{18}O$ values of glass are compared to the average values of the same chondrules from Table 1. The average values for glass in each chondrule are shown in Table 2 for those with multiple glass analyses.

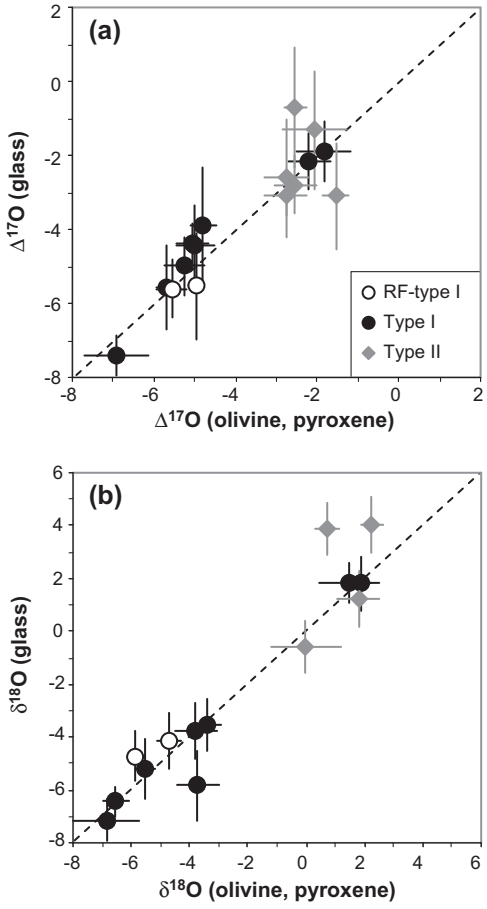

Fig. 9. Comparison of (a) $\Delta^{17}O$ and (b) $\delta^{18}O$ between average oxygen isotope ratios of phenocrysts (olivine and low-Ca pyroxene) and glass in the same chondrules. The close correlation to the dashed 1:1 lines indicates that both glass and phenocrysts often have consistent values within analytical uncertainties. Error bars are 95% confidence (see also Table 2).

Both $\Delta^{17}O$ and $\delta^{18}O$ values of glasses in each chondrule from Acfer 094 are almost identical to those of phenocrysts in each chondrule. These correlations indicate that chondrule glasses are in isotopic equilibrium with olivine and pyroxene phenocrysts at high temperature. Although deviation from the 1:1 line of $\delta^{18}O$ values for a few chondrules might be the result of kinetic effects (evaporation and condensation) during chondrule formation, this is minor for most chondrules. Thus, we confirm that the average oxygen isotope ratios calculated from olivine and low-Ca pyroxene phenocrysts represent oxygen isotope ratios of "relict olivine-free" portion of individual chondrules in Acfer 094. Hereafter, we call this "relict olivine-free" portion of chondrule that consists of multiple mineral phases and glass with indistinguishable $\Delta^{17}O$ values to be the "host chondrule". In contrast, oxygen isotope ratios of "bulk" chondrules are different from those of "host chondrules" if the chondrules contain a number of relict olivine grains.

4.3. A correlation between O isotopes and Mg# of chondrules

Fig. 10 shows distributions of oxygen isotope ratios of host chondrules. In contrast to the large variation among oxygen isotope ratios in relict olivine grains (Fig. 3e–h), oxygen isotope ratios of host chondrules are bimodally distributed within two groups centered between the CCAM line and the Young and Russell line (Fig. 10a). The data cluster in two regions: $\delta^{18}O \sim -5‰$ ($\Delta^{17}O \sim -5‰$) and at $\delta^{18}O \sim 1‰$ ($\Delta^{17}O \sim -2‰$) showing a gap of $\delta^{18}O$ values from $-3‰$ to $0‰$ with only a few exceptions: $\delta^{18}O \sim 3‰$ ($\Delta^{17}O \sim 0‰$) and $\delta^{18}O \sim -12‰$ ($\Delta^{17}O \sim -9‰$) (Fig. 10a and c). The distribution of $\Delta^{17}O$ values of host chondrules from Acfer 094 is similar to that of MgO-rich olivine analyses from primitive chondrites (Libourel and Chaussidon, 2011). The two major groups ($\Delta^{17}O \sim -5‰$ and $\sim -2‰$) show a correlation with mineral chemistry of olivine and pyroxene. The relatively ^{16}O-rich group ($\Delta^{17}O = -5.4 \pm 1.2‰$, 2SD, $n = 19$) consists of chondrules with MgO-rich olivine and pyroxene (Mg# > 96). In contrast, the ^{16}O-poor group ($\Delta^{17}O = -2.2 \pm 0.7‰$, 2SD, $n = 16$) shows wide variation in Mg# and mainly consists of chondrules with more FeO-rich olivine and pyroxene (Mg# ~ 99–42) (Fig. 10b). These two groups exist regardless of chondrule type, i.e., porphyritic chondrules and non-porphyritic chondrules as well as the Al-rich chondrule. Note that G64, which is the most MgO-rich chondrule of the ^{16}O-poor group chondrule ($\Delta^{17}O = -1.83 \pm 0.66‰$, Mg# ~ 99), has relict dusty olivine grains with $\Delta^{17}O$ of ~0‰ (Fig. 7l, Table EA2-3, Fig. EA3).

A similar bimodal distribution has been observed in chondrules and isolated olivine grains from ALHA77307 (CO3) (Jones et al., 2000; Wasson et al., 2004), Murchison (CM2) (Jabeen and Hiyagon, 2003), Acfer 094 (Kunihiro et al., 2005), Y81020 (CO3) (Kunihiro et al., 2004; Tenner et al., 2011), Tagish Lake (C2-ungrouped) (Russell et al., 2010), and CR chondrites (Libourel and Chaussidon, 2011), although Connolly and Huss (2010) reported that type II chondrules from CR2 chondrites tend to have much higher $\Delta^{17}O$ values. The Mg#s of the ^{16}O-rich group chondrules from Acfer 094 are mainly higher than 98 and the lower limit of the occurrence of the ^{16}O-rich group chondrules is at Mg# ~ 96 (Fig. 10b), which is different from that of the petrographic classification of type I and type II chondrules (Mg# = 90). Thus, the ^{16}O-rich group ($\Delta^{17}O \sim -5$) consists of type I chondrules but the ^{16}O-poor group consists of both type I chondrules and type II chondrules. The oxygen isotope ratios of refractory forsterite (RF) bearing type I chondrules ($\Delta^{17}O = -5.0$ to $-6.3‰$) are within the range of those of the ^{16}O-rich group chondrules. This is similar to those of RF-bearing type I chondrules from CV chondrites (Pack et al., 2004).

Table 2
The $\delta^{18}O$ and $\Delta^{17}O$ values of averaged homogeneous phenocrysts and glass in each chondrule.

Chondrule	Type[1]	$\delta^{18}O$		$\Delta^{17}O$	
		Averaged chondrule[2]	Glass[3]	Averaged chondrule[2]	Glass[3]
G56	RF, IAB	-5.86 ± 0.32	-4.71 ± 0.96	-5.55 ± 0.37	-5.61 ± 0.79
G77	RF, IAB	-4.71 ± 0.40	-4.12 ± 1.06	-4.98 ± 0.19	-5.53 ± 1.42
G7	IAB	-3.39 ± 0.49	-3.55 ± 0.99	-5.06 ± 0.38	-4.40 ± 0.57
G26	IAB	-5.53 ± 0.31	-5.20 ± 1.16	-4.99 ± 0.46	-4.41 ± 1.05
G38	IAB	-3.73 ± 0.74	-5.84 ± 1.29	-4.79 ± 0.31	-3.91 ± 1.57
G48	IA, BO	-3.78 ± 0.72	-3.75 ± 1.04	-5.28 ± 0.49	-4.98 ± 0.78
G52	IA	1.88 ± 0.36	1.81 ± 1.04	-2.19 ± 0.51	-2.16 ± 0.78
G64	IB	1.48 ± 1.01	1.83 ± 0.73	-1.83 ± 0.66	-1.90 ± 0.81
G70	IAB	-6.54 ± 0.44	-6.45 ± 0.58	-5.70 ± 0.22	-5.57 ± 1.14
G90	I, Silica	-6.86 ± 1.12	-7.13 ± 0.76	-6.91 ± 0.79	-7.41 ± 0.56
G10	IIA	-0.03 ± 1.20	-0.59 ± 0.99	-2.78 ± 0.53	-3.06 ± 0.57
G32	II,Ol-frag	2.26 ± 0.36	4.00 ± 1.06	-2.54 ± 0.29	-0.70 ± 1.60
G34	IIA	1.79 ± 0.71	1.21 ± 1.06	-2.75 ± 0.53	-2.60 ± 1.60
G35	IIAB	–	1.25 ± 1.06	-2.07 ± 0.80	-1.32 ± 1.60
G63	IIA	0.72 ± 0.39	3.88 ± 0.96	-2.54 ± 0.50	-2.79 ± 0.79
G79	IIAB	–	3.47 ± 1.06	-1.54 ± 0.32	-3.11 ± 1.42

[1] RF = refractory forsterite bearing, I = type I, II = type II, A = predominately olivine phenocrysts, AB = olivine and pyroxene phenocrysts, BO = barred olivine, Silica = silica-bearing, Ol-frag = olivine fragment.
[2] Averaged values of homogeneous phenocrysts.
[3] Averaged value is shown if multiple data exist.

Interestingly, if we calculate the average $\Delta^{17}O$ of cometary chondrule-like objects from the comet Wild 2 using oxygen isotope data of pyroxenes of individual objects (excluding one anomalous pyroxene analysis of Torajiro; Nakamura et al., 2008) according to the concept of host chondrules, their average $\Delta^{17}O$ value is $\sim -2‰$ with Mg# of 96–86 (Fig. 10b), which is consistent with the ^{16}O-poor group from Acfer 094.

5. DISCUSSION

5.1. Oxygen isotope ratios of the chondrule-forming melt

5.1.1. Oxygen isotopic compositions of phenocrysts and glass

Most porphyritic chondrules studied in this work consist largely of olivine and low-Ca pyroxene phenocrysts, and fine-grained minerals and glass in mesostasis that show identical $\Delta^{17}O$ values, which we interpret to be the host chondrule. Fig. 11 shows $\delta^{18}O$ values of olivine and low-Ca pyroxene phenocrysts of individual host chondrules. Chaussidon et al. (2008) suggested that olivine in type I chondrules are derived from differentiated planetesimals and that oxygen isotope ratios of olivine and pyroxene in type I chondrules from CV and CR chondrites record a mixing trend between ^{16}O-rich olivine and ^{16}O-poor SiO gas in the Solar Nebula. The suggested trend ($\delta^{18}O(\text{pyroxene}) = 0.72 \times \delta^{18}O(\text{olivine}) + 1.21$) by Chaussidon et al. (2008) is shown as a dashed line labeled C08 in Fig. 11. In contrast, our data are distributed on the 1:1 line and are not consistent with the trend of C08. Recently, Rudraswami et al. (2011) reported that oxygen isotope ratios of olivine and low-Ca pyroxene of individual chondrules from Allende (CV3) are also distributed on the 1:1 line. We do not find any data along the trend reported by Chaussidon et al. (2008) or evidence to support the planetesimal origin for olivine grains in chondrules. Instead, oxygen isotope data of both this study and Rudraswami et al. (2011) suggest that most of the olivine and pyroxene in each chondrule crystallized from the same chondrule-forming melt.

Considering that olivine has the highest liquidus temperature among the constituent minerals in ferromagnesian chondrules, it is possible that some olivine grains in porphyritic chondrules remained solid during the chondrule-melting processes (e.g., Connolly and Desch, 2004). If residual olivine had distinct oxygen isotope ratios from the chondrule-forming melt, their oxygen isotope ratios could be preserved due to the short time-scales involved and slow diffusion of oxygen in olivine (Jaoul et al., 1980; Houlier et al., 1988). Oxygen isotope ratios of remaining minerals and glass may represent those of the chondrule-forming melt. Next, we will discuss characteristics of oxygen isotope ratios of host chondrules. Characteristics of oxygen isotope ratios of relict olivine grains, which may preserve information of precursor of chondrules, will be discussed in Section 5.3.

We found that phenocrysts and coexisting glass have identical $\Delta^{17}O$ values at the level of $1‰$ in a large number of chondrules from Acfer 094 (Fig. 9). This is distinct from previously reported data. In the previous studies from type 3 carbonaceous and ordinary chondrites, the $\Delta^{17}O$ values of glass or mesostasis in chondrules are significantly higher

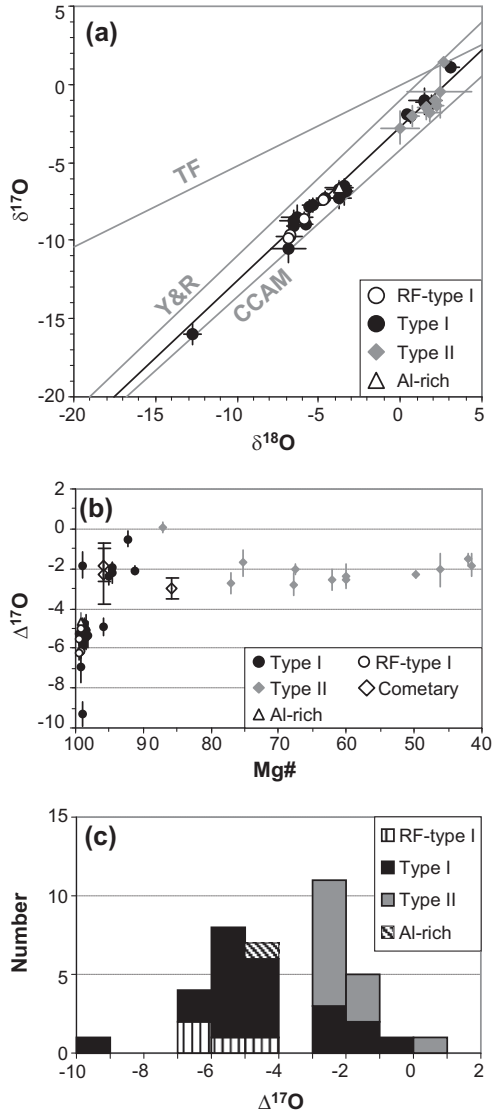

Fig. 10. (a) Oxygen three-isotope plot of average values of individual host chondrules and olivine fragments (see Table 1 and Table EA2-3). Error bars are 95% confidence. Four reference lines are the same as Fig. 3. (b) Average $\Delta^{17}O$ values plotted vs. Mg# for individual host chondrules and olivine fragments. For comparison, the average $\Delta^{17}O$ values of pyroxene from chondrule-like objects (data from Nakamura et al., 2008) are shown as "Cometary". Error bars are 95% confidence (see Electronic Annex EA1). (c) Histogram of the average $\Delta^{17}O$ of individual host chondrules and olivine fragments showing a bimodal distribution of oxygen isotope ratios.

than those of phenocrysts (Bridges et al., 1999; Maruyama et al., 1999; Maruyama and Yurimoto, 2003; Chaussidon et al., 2008; Kita et al., 2010). For instance, Kita et al. (2010) observed higher $\Delta^{17}O$ and $\delta^{18}O$ values in glass relative to those of phenocrysts in the same chondrules from the least equilibrated ordinary chondrite, Semarkona (LL3.01 after Kimura et al., 2008). The $\Delta^{17}O$ values of glass in Semarkona were as high as $5‰$, which is similar to those in matrix magnetite that formed by the aqueous alteration in the LL chondrite parent body (Choi et al., 1997). For this

reason, Kita et al. (2010) concluded that oxygen isotope ratios in chondrule glass in Semarkona were altered by isotope exchange with aqueous fluid at low temperature in the parent body. In contrast, Acfer 094 did not experience any thermal metamorphism or aqueous alteration in the parent body, based on occurrence of martensite in chondrules (Kimura et al., 2008), highly unequilibrated fine-grained matrix (Greshake, 1997), and fine-grained cosmic symplectite (COS) in matrix (Sakamoto et al., 2007). Therefore, we consider that glass in Acfer 094 chondrules preserves the pristine oxygen isotope ratios of chondrule-forming melt at the time when chondrules solidified.

Almost all "primitive chondrites" would have experienced parent body processes to some extent that might disturb their pristine oxygen isotope ratios in chondrule mesostasis. In type 3 chondrites such as LL3 and CV3, that were slightly more altered or metamorphosed in their parent bodies than Semarkona, oxygen isotope ratios in plagioclase and silica might have been altered by exchange with fluid due to fast oxygen isotope diffusivities in those minerals (Cole and Chakraborty, 2001). High-Ca pyroxene would be overgrown during devitrification of glass and replacement of plagioclase by nepheline (Brearley and Jones, 1998; Huss et al., 2006), during which isotope exchange would occur. In type 2 chondrites such as CM2 and CR2, minerals and glass might have been replaced by alteration products such as phyllosilicates (Brearley, 2006) and intrinsic oxygen isotope ratios could be disturbed. In these cases, it is difficult to determine oxygen isotope systematics of individual chondrules. However, oxygen isotope data in Acfer 094 chondrules show that the $\Delta^{17}O$ values of low-Ca pyroxene and of most olivine phenocrysts are in good agreement with those of minerals and glass in chondrule mesostasis (e.g., Fig. 3j and k). Similarly, a few analyses of high-Ca pyroxene in Semarkona are also indistinguishable from olivine and low-Ca pyroxene in the same chondrules (Kita et al., 2010). Thus, oxygen isotope ratios of host chondrules can be represented by those in phenocrysts, especially low-Ca pyroxene, which should have been crystallized from melt and would easily preserve their primary oxygen isotope signature against mild parent body processes. The high precision and accuracy of SIMS oxygen isotope analysis of multiple olivine and low-Ca pyroxene phenocrysts in a single chondrule would be very useful way to characterize oxygen isotope ratios of chondrules. This approach can be applied to chondrules in many different chondrites even if they have suffered parent body alteration in some degree.

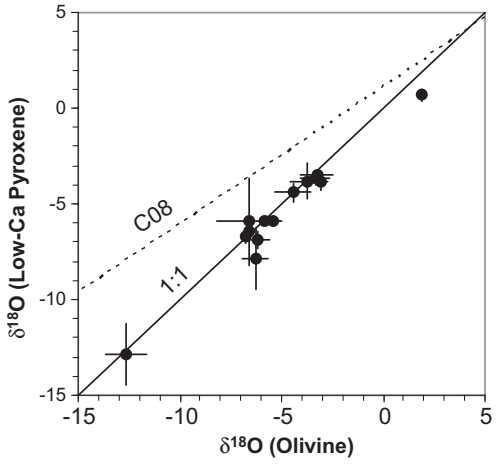

Fig. 11. Comparison of average $\delta^{18}O$ values between olivine and coexisting low-Ca pyroxene. The 1:1 line (solid line) and the previously reported correlation line in chondrules by Chaussidon et al. (2008) (dotted line, C08) are shown. Error bars are 2SD of oxygen isotope data of individual chondrules (Table EA2-3).

5.1.2. Mechanisms for oxygen isotopic homogeneity of the chondrule-forming melt

A host chondrule with internally homogeneous $\Delta^{17}O$ values from multiple mineral phases and glass strongly indicates that the chondrule-forming melt had homogeneous oxygen isotope ratios and remained unchanged during and after cooling. Our data do not support zoning of $\Delta^{17}O$ values in the chondrule-forming melt, which has been hypothesized as a result of a partial oxygen isotope exchange between gas and the chondrule-forming melt having distinct $\Delta^{17}O$ values (e.g., Clayton et al., 1983).

If we assume that chondrule formation was in a closed system for oxygen isotope exchange with surrounding gas, then oxygen isotope ratios in a chondrule were homogenized to be an average value of heterogeneous precursor dusts, excluding relict olivine grains. However, many chondrules might be formed in an open system with respect to major oxides, such as MgO and SiO_2, and recondensed from surrounding gas (e.g., Libourel et al., 2006; Nagahara et al., 2008). Furthermore, in a given chondrule, the "homogenized" host chondrule's $\Delta^{17}O$ value is always at the higher or lower end of the $\Delta^{17}O$ distribution among relict olivine grains (e.g., Fig. 3e–g). As we observed a wide range of $\Delta^{17}O$ values among relict olivine grains in Acfer 094 chondrules (from −23 to 0‰), it is odd that we do not observe intermediate $\Delta^{17}O$ values in host chondrules with respect to those of relict olivine grains in the same chondrules.

Based on an experimental study of oxygen isotope exchange between water vapor and chondrule-forming melt, Yu et al. (1995) predicted the occurrence of internal oxygen isotope zoning in the chondrule-forming melt due to partial oxygen isotope exchange at low H_2O partial pressures, the canonical condition of the solar nebula. Assuming this condition, the observed internal oxygen isotope homogeneity in Acfer 094 chondrules indicates that they formed in environments where solar nebula gas and precursor solid had identical isotope ratios. Alternatively, if chondrules formed in dust-enriched environments (Ebel and Grossman, 2000; Ozawa and Nagahara, 2001; Alexander, 2004; Alexander et al., 2008; Nagahara et al., 2008), isotope exchange between ambient gas and the chondrule-forming melt might have occurred rapidly due to evaporation and re-condensation of major silicates during the chondrule-forming high temperature heating events. In this case, the oxygen isotope ratios in the temporal gas would be the same as average precursor solids, so that repeated chondrule-forming events would result in homogeneous local oxygen isotope reservoirs. In addition, if the chondrule-forming melt was formed by frictional heating in a shocked nebular gas

(Desch et al., 2005), internal flow of the melt (Uesugi et al., 2003) would enhance homogenization of oxygen isotopes of the melt. Thus, oxygen isotope ratios of host chondrules represent those of chondrule-forming region.

5.2. Two major oxygen isotope reservoirs in Acfer 094 chondrule-forming regions

The $\Delta^{17}O$ values of host chondrules from Acfer 094 show a bimodal distribution ($\Delta^{17}O \sim -5‰$ and $-2‰$) with only a few exceptions (Fig. 10c). This indicates that these chondrules mostly formed in two distinct oxygen isotope reservoirs. The ^{16}O-rich chondrules ($\Delta^{17}O \sim -5‰$) consist of phenocrysts of low FeO content (Mg# > 96), implying that they formed under a reducing environment. In contrast, the ^{16}O-poor chondrules with a nearly constant $\Delta^{17}O$ value of $-2‰$ have a wide range of FeO contents (Mg# ~ 99 with metal grains to Mg# ~ 42, Fig. 10b). Mg# is controlled by a number of factors, including bulk composition, but for a single composition, oxygen fugacity is most important. The occurrence of such a wide range in composition from Mg# ~ 99 to 42 indicates that they formed under a wide range of oxygen fugacity ($\log f(O_2)$) from −11 to −9 at 1600 °C) (Zanda et al., 1994), which corresponds to ~IW-3 to IW-1, below the Iron–Wustite (IW)-buffer (Myers and Eugster 1983).

The relation between Mg# and the $\Delta^{17}O$ value of chondrules suggests that an increase of the $\Delta^{17}O$ value of chondrules is closely associated with oxidation of the ambient nebular gas, which may be linked to the processing of ices and icy bodies (Connolly and Huss, 2010). However, if the oxygen fugacity of the chondrule forming environment was simply controlled by the addition of water or ice with an extremely high $\Delta^{17}O$ value, which is the predicted component from a CO self-shielding model (Yurimoto and Kuramoto, 2004) and could be as high as $\Delta^{17}O = +80‰$ (inferred from COS in Acfer 094 matrix, Sakamoto et al., 2007), the $\Delta^{17}O$ values in chondrule hosts should strongly correlate with Mg#. This is not the case for chondrules in Acfer 094 because the $\Delta^{17}O$ values of ~−2‰ are seen from chondrules independent of their Mg#. The extremely ^{16}O-poor water predicted from CO self-shielding might have contributed an oxygen isotope reservoir for the ^{16}O-poor group chondrules by mixing of more ^{16}O-rich dusts, such as precursors of CAIs and AOAs ($\Delta^{17}O \sim -25‰$) or the ^{16}O-rich group chondrules ($\Delta^{17}O \sim -5‰$). However, if this is the case, an increase of $\Delta^{17}O$ value and an exchange of oxygen isotopes between the extremely ^{16}O-poor water and silicate dust in the chondrule-forming region must have occurred prior to chondrule formation. Instead, the fairly constant $\Delta^{17}O$ among these ^{16}O-poor group chondrules could be explained by formation in a dust-rich environment (Wood and Hashimoto, 1993; Ebel and Grossman, 2000; Alexander, 2004; Fedkin and Grossman, 2006) if the oxygen fugacity varied according to the degree of dust enrichment. Alternatively, the oxygen fugacity may also increase with abundance of water or ice whose $\Delta^{17}O$ value was close to that of the precursors of the ^{16}O-poor group chondrules.

The two major oxygen isotope reservoirs ($\Delta^{17}O = -5‰$ and $-2‰$) that are recognized in chondrules from Acfer 094 may have existed commonly and broadly in the early solar system. In the Acfer 094 meteorite, more than 50% of chondrules are in the ^{16}O-rich group ($\Delta^{17}O \sim -5‰$). This is deduced because type I chondrules comprise 80% of chondrules in Acfer 094 (Kunihiro et al., 2005) and 18 out of 25 type I chondrules (excluding "heterogeneous" chondrules) are classified into the ^{16}O-rich group in this study. The existence of these two chondrule groups in carbonaceous chondrites is supported by published data although these groups were not previously recognized. The ^{16}O-rich group ($\Delta^{17}O \sim -5‰$) seems to be abundant in CV and CO chondrites (Rubin et al., 1990; Maruyama et al., 1999; Jones et al., 2000, 2004; Wasson et al., 2004; Chaussidon et al., 2008, 2010; Jones and Schilk, 2009; Libourel and Chaussidon, 2011). The ^{16}O-poor chondrules ($\Delta^{17}O \sim -2‰$) are commonly observed in CR, CH, and CB_b chondrites (Krot et al., 2006a,b, 2010; Nakashima et al., 2010, 2011a; Libourel and Chaussidon, 2011). Bimodal distribution of $\Delta^{17}O$ values among chondrules similar to those in this study have been observed from Allende (CV3) and Y 81020 (CO3.0) chondrites (Rudraswami et al., 2011; Tenner et al., 2011). The $\Delta^{17}O$ values of some anhydrous interplanetary dust particles (IDPs) (Aléon et al., 2009), and of chondrule-like objects and low-Ca pyroxene fragments recovered from the comet Wild 2 (McKeegan et al., 2006; Nakamura et al., 2008; Nakashima et al., 2011b) are also clustered around $-2‰$. These results suggest that the environment where the ^{16}O-poor chondrule group ($\Delta^{17}O \sim -2‰$) formed existed at the outer asteroid belt or beyond and that chondrules and crystalline silicates formed there were widely distributed throughout the outer solar nebula, from the outer asteroid belt to the Kuiper belt region.

The study on the Al–Mg systematics of some of chondrules in Acfer 094 does not show a correlation between inferred initial $^{26}Al/^{27}Al$ ratios and $\Delta^{17}O$ values (Ushikubo et al., 2010). Tenner et al. (2011) measured oxygen isotope ratios of chondrules in Y 81020 (CO3.0) that were previously analyzed for Al–Mg age (Kurahashi et al., 2008) and showed no correlation between inferred initial $^{26}Al/^{27}Al$ ratios and $\Delta^{17}O$ values. The absence of correlation between $\Delta^{17}O$ values and ^{26}Al ages of chondrules in a single meteorite suggests that chondrules record regional oxygen isotopic heterogeneity in the chondrule-forming regions of the solar nebula instead of a temporal change of oxygen isotope ratios in the solar nebula. This is similar to the suggestion by Kurahashi et al. (2008) based on the contemporaneous formation of chondrules in LL3 and CO3 chondrites that have distinct oxygen isotope ratios. Different chondritic parent bodies probably collected different fractions of chondrules that have various oxygen isotope ratios. Furthermore, minor chondrule groups that have distinct $\Delta^{17}O$ values (e.g., ~−9‰, ~0‰, and ~1‰) have been recognized in carbonaceous chondrites (Connolly and Huss, 2010; Nakashima et al., 2010, 2011a; Libourel and Chaussidon, 2011), some of which were identified among Acfer 094 chondrules. Highly precise and accurate oxygen isotope ratios of "host chondrules" will determine the distribution of oxygen isotopes in the solar nebula before chondrules accreted into their parent bodies.

5.3. Relict olivine grains and oxygen isotope reservoirs

In this study, nearly half of the chondrules contain relict olivine grains that show either relatively ^{16}O-rich or ^{16}O-poor oxygen isotope ratios relative to the host chondrules (Fig. 12). In four chondrules, significantly ^{16}O-enriched olivine grains with Δ^{17}O values lower than $-10‰$ (down to $-23‰$) are observed (G45, G68, G70, and G84; Figs. 3f,h, 6b and 7i, Table EA2-3), similar to those reported in other chondrites (e.g., Yurimoto and Wasson, 2002; Jones et al., 2004). Precursors of these olivine grains could be uniformly ^{16}O-enriched olivine-bearing inclusions, such as amoeboid olivine aggregates (AOA) (e.g., Hiyagon and Hashimoto, 1999; Aléon et al., 2002; Krot et al., 2002; Kobayashi et al., 2003; Fagan et al., 2004; Itoh et al., 2007). In the previous studies, heterogeneous oxygen isotope ratios in chondrules are interpreted as the result of mixing of ^{16}O-rich solid precursor and ^{16}O-poor nebula gas (e.g., Clayton et al., 1983; Krot et al., 2005). Under this simple mixing model, relict olivine grains should be always more ^{16}O-rich than host chondrules. Many chondrules have ^{16}O-rich relict olivine grains relative to oxygen isotope ratios of host chondrules. However, four type I chondrules in Acfer 094 have the reverse relation; ^{16}O-poor relict grains are observed (Fig. 12). In addition, most relict grains have Δ^{17}O values between $-2‰$ and $-6‰$, and fully overlap with the two major isotope reservoirs discussed above. Many ^{16}O-poor relict olivine grains are observed in ^{16}O-rich group chondrules and vice versa (Fig. 12). These data suggest that the majority of relict olivine grains are not related to AOA-like precursors, but instead relate to materials formed in two major isotope reservoirs. Thus migration of solid precursor might have occurred from one isotope reservoir to the other before the melting of chondrules. The results from this study suggest that distinct oxygen isotope reservoirs existed in the protoplanetary disk at the time of chondrule formation (2–3 Ma after CAI formation; Kita et al., 2005) although their spatial and time scales are not known. A limited amount of radial migration might occur between separated disk regions (Cuzzi et al., 2010), which resulted in limited range of the Δ^{17}O values among relict olivine grains in many chondrules. Mixing of different isotope reservoirs seems to occur between ordinary-chondrite forming regions and carbonaceous-chondrite forming regions (Kita et al., 2010). Some chondrules in LL chondrites are significantly ^{16}O-rich with Δ^{17}O values as low as $-9‰$ (Russell et al., 2000; Ruzicka et al., 2007; Kita et al., 2010), similar to those found in MgO-rich type I chondrules (Mg# > 96) in Acfer 094 and other chondrules in carbonaceous chondrites. Kita et al. (2010) further suggested that type II chondrules in LL3 are on the mixing line between ordinary chondritic precursors ($\Delta^{17}O \geqslant 1.6‰$) and CV chondrite BO chondrule-like precursors ($\Delta^{17}O \sim -2‰$). Weisberg et al. (2011) reported that some chondrules from E3 chondrites contain minerals whose oxygen isotope ratios are similar to those of chondrules from ordinary, carbonaceous, and R chondrites.

Although a secular change of oxygen isotope ratios of the ambient nebular gas in the individual chondrule forming region might have occurred during the chondrule-forming process (e.g., Connolly and Huss, 2010), the occurrence of multiple oxygen isotope components in chondrules from various types of chondrite suggests that migration of chondrules and chondrule precursor silicates was common in chondrule forming regions. Host chondrules preserve chemical and isotopic characteristics of the last chondrule formation that occurred in different regions of the protoplanetary disk. As described in the Section 5.2, more than 50% of chondrules in Acfer 094 are the ^{16}O-rich group ($\Delta^{17}O \sim -5‰$). The materials accreted to the Acfer 094 parent asteroid were mainly from the region with $\Delta^{17}O \sim -5‰$, while a smaller portion also derived from the region with the Δ^{17}O value $\sim -2‰$.

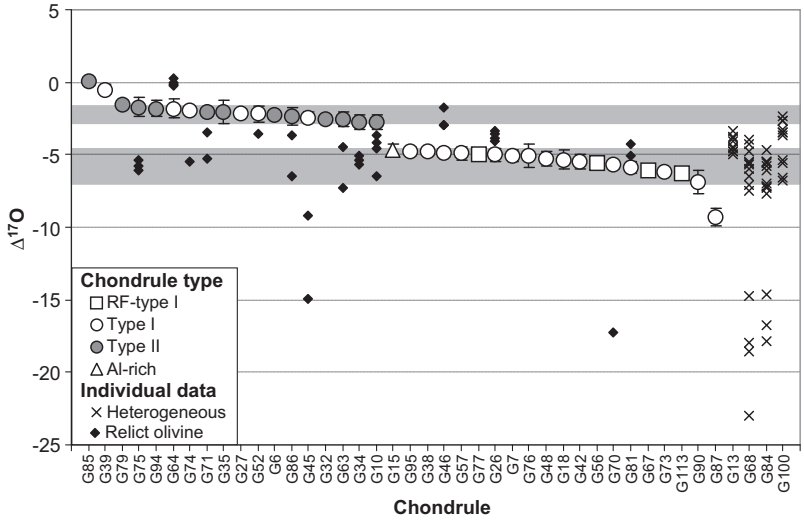

Fig. 12. The Δ^{17}O values of host chondrules, relict olivine grains, and individual minerals in heterogeneous chondrules. The gray bands represent the range of two major chondrule groups reported in this study (the ^{16}O-rich group and the ^{16}O-poor group). Chondrule data are sorted in the order of the Δ^{17}O values. Error bars are 95% confidence.

5.4. Primary oxygen isotope trend in chondrules

Oxygen isotope ratios of chondrules from Acfer 094 are distributed between the CCAM (Clayton et al., 1977) and Y&R lines (Young and Russell, 1998) (Fig. 10a). To characterize oxygen three-isotope systematics of anhydrous minerals in chondrules from the least metamorphosed carbonaceous chondrite, we plot individual oxygen isotope analyses obtained in this work as shown in Fig. 13. We used only data from olivine and low-Ca pyroxene measured with the high-intensity 15 μm beam because: 1) analyses with a high intensity beam provide the highest precision and accuracy and 2) olivine and low-Ca pyroxene are major phenocrysts of chondrules that would not significantly fractionate oxygen isotopes during igneous differentiation. The data are tightly clustered along a slope ~1 line from $\delta^{18}O = -43.4 \pm 0.3‰$ to $3.1 \pm 0.2‰$. These data are distinct from, and plot between the CCAM line and the Y&R line (Fig. 13). The regression line of these data is $\delta^{17}O = (0.987 \pm 0.013) \times \delta^{18}O - (2.70 \pm 0.11)$ (95% confidence, MSWD = 5.0). We also found that oxygen isotope ratios measured at WiscSIMS of olivine and low-Ca pyroxene in chondrules from CH, CO, and CV chondrites are consistently distributed along this regression line (Nakashima et al., 2011a; Rudraswami et al., 2011; Tenner et al., 2011). Thus, we interpret the new line obtained from olivine and low-Ca pyroxene phenocrysts of chondrules in this study to represent the best estimate for anhydrous minerals of chondrules that formed in the solar nebula. Here, we call this line the Primitive Chondrule Minerals (PCM) line.

Our data are generally similar to bulk CV3 chondrules (Clayton et al., 1983; Rubin et al., 1990; Jones et al., 2004), but systematically plot towards the left (depleted in ^{18}O) from bulk CV3 chondrules (Fig. 13a). It is possible that the bulk chondrule data are biased to heavy isotope enrichment along slope ~0.5 mass fractionation lines because aqueous alteration in CV3 chondrite parent body would result in higher $\delta^{18}O$ in altered mesostasis in chondrules (Bridges et al., 1999; Young et al., 2002; Kita et al., 2010; Rudraswami et al., 2011).

The slope of the PCM line (0.987 ± 0.013) is slightly steeper than the CCAM line (0.94), but indistinguishable from unity within uncertainty. This line intersects the terrestrial fractionation (TF) line at $\delta^{18}O = 5.8 \pm 0.4‰$, which is indistinguishable from the value for the terrestrial mantle ($\delta^{18}O = 5.5‰$) (Eiler, 2001), lunar rocks (Wiechert et al., 2001; Spicuzza et al., 2007) and bulk enstatite chondrites (Clayton, 2003; Franchi, 2008). Furthermore, oxygen isotope ratios of extremely ^{16}O-poor COS in the matrix of the Acfer 094 meteorite (Sakamoto et al., 2007) plot on the extension of the PCM line within uncertainty (Fig. 13b inset). Oxygen isotope ratios of the most ^{16}O-rich CAIs and a chondrule from carbonaceous chondrites (Kobayashi et al., 2003; Gounelle et al., 2009) are also consistent with the PCM line, although the precision of these data are not high enough to distinguish the difference between the CCAM line and the PCM line (Fig. EA1-2 in Electronic Annex EA1).

A simple trend line cannot explain the variation of oxygen isotope ratios of planetary materials. For example,

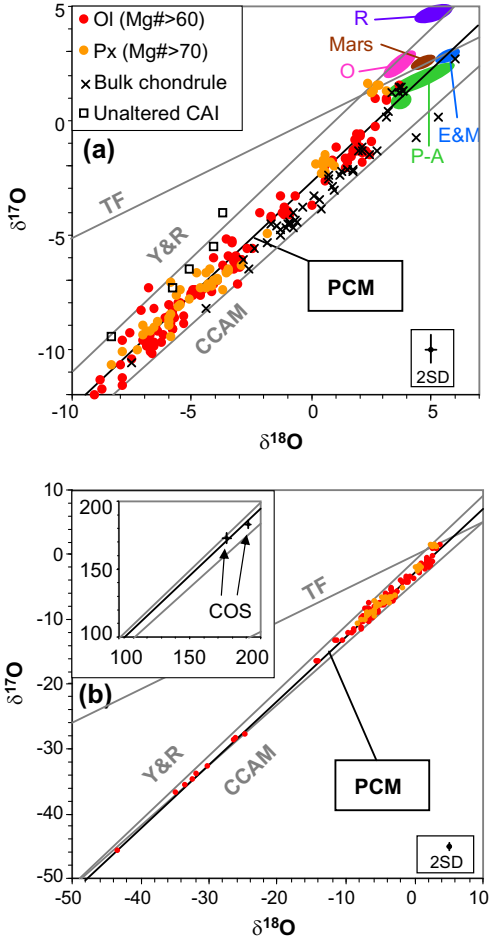

Fig. 13. Oxygen isotope ratios of olivine (Mg# > 60) and pyroxene (Mg# > 70) phenocrysts of chondrules and olivine fragments from Acfer 094 (individual *in situ* analyses, with a 15 μm spot). (a) Enlarged view of oxygen isotope ratios of individual analyses. For comparison, oxygen isotope ratios of bulk chondrules from CV chondrite (Clayton et al., 1983; Jones et al., 2004), those of unaltered CAI (Young and Russell, 1998), and those of Earth and Moon (E&M), Martian meteorites (Mars), most primitive achondrites (P-A), ordinary chondrite (O), and R chondrite (R) (Clayton, 2003) are shown. (b) Overall view of oxygen isotope ratios of individual analyses. In the inset, oxygen isotope data of cosmic symplectites (COS) with *in situ* SIMS analyses (Sakamoto et al., 2007) are shown. Four reference lines are the same as Fig. 3. Typical uncertainty (2 SD) of 15 μm spot analyses is shown at the lower-right of each panel.

although oxygen isotope ratios of most primitive achondrites, such as lodranites, acapulcoite, winoanites, and brachinites plot close to the PCM line, other achondrites such as HED meteorites, Ureilites, and Martian meteorites are not on the PCM line (Clayton, 2003; Franchi, 2008) (Fig. 13a). The apparent exceptions to the PCM line are chondrules from ordinary and R chondrites whose oxygen isotope ratios are distributed to the left of the PCM line (Fig. 13a). However, Kita et al. (2010) found that oxygen three isotope ratios of some chondrules and relict olivine grains in chondrules from Semarkona (LL3.0) plot between the CCAM line and the Y&R line with negative $\Delta^{17}O$

values, similar to those in carbonaceous chondrites. Similarly, oxygen isotope ratios of ^{16}O-rich olivine grains in chondrules from enstatite chondrites plot along a slope 1 line that is indistinguishable from the PCM line (Weisberg et al., 2010, 2011). The data for these relict olivine grains suggest that the precursor of at least some chondrules from ordinary and enstatite chondrites consisted of dust whose oxygen isotope ratios were similar to those of chondrules from carbonaceous chondrites. An additional process is needed to cause lighter oxygen isotope ratios of chondrules from ordinary and R chondrites.

Clayton et al. (1991) pointed out that silicates favor enrichment of lighter oxygen isotopes by a few ‰ in δ^{18}O compared to CO and H_2O gas under equilibrium at high temperatures (~1500°C). The equilibrium oxygen isotope fractionation factor between dust and gas is variable according to partial pressure of gas species (e.g., CO, H_2O) and the gas/dust ratio (Onuma et al., 1972; Kita et al., 2010). Kita et al. (2010) observed systematic variations in δ^{18}O among type I chondrules in Semarkona (LL3) that inversely correlate with Mg/Si ratios of chondrules, which they interpreted as isotope fractionation between gas and solid during chondrule formation. It is possible that the deviation of oxygen isotope ratios of chondrules from ordinary and R chondrites from the PCM line might reflect gas–solid isotope fractionation prior to or during chondrule forming processes. Conversely, the PCM line with a slope ~1.0 may represent the mixing of two extreme oxygen isotope reservoirs in the protoplanetary disk, such as those represented by COSs and CAIs. Early processes occurred in the solar nebula which resulted in the mixing of extreme reservoirs and formed dust particles with oxygen isotope ratios along the PCM line. These dust particles might be precursors of chondrules and the ranges of Δ^{17}O values in dust would be locally homogenized in the dust-enriched disk during chondrule formation.

6. CONCLUSIONS

We performed *in situ* oxygen three-isotope analyses of minerals and glass in chondrules from Acfer 094, which is one of the least equilibrated carbonaceous chondrites, to understand systematics of oxygen isotopes in chondrules. The main conclusions obtained from this study are:

(1) Most chondrules in Acfer 094 (38 out of 42) mostly consist of minerals and glass that are isotopically homogeneous within each chondrule with indistinguishable Δ^{17}O values which we call the “host chondrule”. Host chondrules crystallized from a melt with homogeneous Δ^{17}O values that remained unchanged during subsequent cooling of the chondrule-forming melt.

(2) The presence of small amounts of relict olivine with different Δ^{17}O values from the host chondrule demonstrates the usefulness of multiple high precision isotope analyses of olivine and low-Ca pyroxene in a single chondrule to estimate the pristine oxygen isotope ratios in the chondrule-forming melt.

(3) Most chondrules in Acfer 094 are divided into two oxygen isotope groups, the ^{16}O-rich group ($\Delta^{17}O = -5.4 \pm 1.2$‰, 2SD, $n = 19$ with Mg# > 96) and the ^{16}O-poor group ($\Delta^{17}O = -2.2 \pm 0.7$‰, 2SD, $n = 16$ with Mg# ~ 99–42), indicating that these chondrules formed in two distinct oxygen isotope reservoirs in the solar nebula. The ^{16}O-poor chondrule group ($\Delta^{17}O \sim -2$‰) in Acfer 094 may relate to the common occurrence of the ^{16}O-poor chondrules ($\Delta^{17}O \sim -2$‰) in carbonaceous chondrites and the comet Wild 2. Therefore, we suggest that the environment where the ^{16}O-poor chondrule group ($\Delta^{17}O \sim -2$‰) formed existed at the outer asteroid belt or beyond and that chondrules and crystalline silicates formed there were widely distributed throughout the outer solar nebula, from the outer asteroid belt to the Kuiper belt region.

(4) The Δ^{17}O values of relict olivine grains in chondrules from Acfer 094 mainly distribute from −2 to −6‰, which corresponds to the range of Δ^{17}O values of the ^{16}O-rich and ^{16}O-poor chondrule groups. This suggests that the precursor solids of chondrules from Acfer 094 migrated between the locations of two isotope reservoirs.

(5) Oxygen isotope ratios of minerals in chondrules from Acfer 094 are distributed along a slope ~1 line ($\delta^{17}O = (0.987 \pm 0.013) \times \delta^{18}O - (2.70 \pm 0.11)$), which we call the Primitive Chondrule Minerals (PCM) line. The PCM line falls between the CCAM and the Y&R lines and intersects the terrestrial fractionation line at $\delta^{18}O = 5.8 \pm 0.4$‰, which is indistinguishable from the value for the terrestrial mantle ($\delta^{18}O = 5.5$‰). We propose that the PCM line represents the primary trend of the major oxygen isotope reservoirs (^{16}O-rich CAIs and ^{16}O-poor COS) in the protoplanetary disk from which chondrules in various chondrite classes were produced.

ACKNOWLEDGEMENTS

We thank Glenn J. MacPherson and Linda Welzenbach, Smithsonian Institute, for the use of the Acfer 094 thin section. We also thank Akira Yamaguchi, NIPR, for the Raman analysis and Jim Kern for the technical support at WiscSIMS laboratory. We thank Alexander N. Krot for editorial handling, and Devin Schrader, Tak Kunihiro, and an anonymous reviewer for constructive reviews. This work is supported by NASA Cosmochemistry Program (NNX07AI46G and NNX10AH77G, N.T.K.) and a Grant-in-aids of Ministry of Education, Science, and Culture (No. 19540500 and 22540488, M.K.). WiscSIMS is partly supported by NSF (EAR03-19230, EAR07-44079, EAR10-53466).

APPENDIX A. SUPPLEMENTARY DATA

Supplementary data associated with this article can be found, in the online version, at http://dx.doi.org/10.1016/j.gca.2012.05.010.

REFERENCES

Aléon J., Engrand C., Leshin L. A. and McKeegan K. D. (2009) Oxygen isotopic composition of chondritic interplanetary dust particles: A genetic link between carbonaceous chondrites and comets. *Geochim. Cosmochim. Acta* **73**, 4558–4575.

Aléon J., Krot A. N. and McKeegan K. D. (2002) Calcium-aluminum-rich inclusions and amoeboid olivine aggregates from the CR carbonaceous chondrites. *Meteorit. Planet. Sci.* **37**, 1729–1755.

Alexander C. M. O'D. (2004) Chemical equilibrium and kinetic constraints for chondrule and CAI formation conditions. *Geochim. Cosmochim. Acta* **68**, 3943–3969.

Alexander C. M. O'D. Grossman J. N., Ebel D. S. and Ciesla F. J. (2008) The formation conditions of chondrules and chondrites. *Science* **320**, 1617–1619.

Brearley A. J. (2006) The action of water. In *Meteorites and the Early Solar Systems II* (eds. D. S. Lauretta and H. McSween Jr.). The University of Arizona Press, Tucson, pp. 587–624.

Brearley A. J. and Jones R. H. (1998) Chondritic meteorites. In *Reviews in Mineralogy & Geochemistry 36, Planetary Materials* (ed. J. J. Papike). Mineralogical Society of America, Washington, DC, pp. 3-1–3-398.

Boesenberg J. S., Hewins R. H. and Chaussidon M. (2004) Oxygen isotopic diffusion and exchange experiments on olivine and chondrule melts: preliminary results. *Workshop on Chondrites and Protoplanetary Disk*, #9049 (abstr.).

Boesenberg J. S., Cosarinsky M., McKeegan K. D., Chaussidon M. and Hewins R. H. (2008) An experimental study of Fe–Mg and oxygen isotope exchange between relict olivine and chondrule melt. *Lunar Planet. Sci.* 38, #1621 (CD-ROM) (abstr.).

Bridges J. C., Franchi I. A., Sexton A. S. and Pillinger C. T. (1999) Mineralogical controls on the oxygen isotopic compositions of UOCs. *Geochim. Cosmochim. Acta* **63**, 945–951.

Chaussidon M., Libourel G. and Krot A. N. (2008) Oxygen isotopic constraints on the origin of magnesian chondrules and on the gaseous reservoirs in the early solar system. *Geochim. Cosmochim. Acta* **72**, 1924–1938.

Chaussidon M., Villenueve J. and Rollion-Bard C. (2010) High precision O isotopic measurements of Mg-rich olivine from the Allende meteorite: constraints on their origin. *Meteorit. Planet. Sci. Suppl.* **45**, A34 (abstr.).

Choi B. G., McKeegan K. D., Leshin L. A. and Wasson J. T. (1998) Extreme oxygen-isotope compositions in magnetite from unequilibrated ordinary chondrites. *Nature* **392**, 577–579.

Ciesla F. J. (2005) Chondrule-forming processes – An overview. In *Chondrites and the Protoplanetary Disk* (eds. A. N. Krot, E. R. D. Scott and B. Reipurth). Astronomical Society of the Pacific, San Francisco, CA, pp. 811–820.

Clayton R. N. (2002) Solar system: self-shielding in the solar nebula. *Nature* **415**, 860–861.

Clayton R. N. (2003) Oxygen isotopes in meteorites. In *Treatise on Geochemistry 1, Meteorites, Comets, and Planets* (ed. A. M. Davis). Elsevier-Pergamon, Oxford, pp. 129–142.

Clayton R. N., Mayeda T. K., Hutcheon I. D., Molini-Velsko C., Onuma N., Ikeda Y. and Olsen E. J. (1983) Oxygen isotopic compositions of chondrules in Allende and ordinary chondrites. In *Chondrules and their Origins* (ed. E. A. King). Lunar Planet. Inst., Houston, TX, pp. 37–43.

Clayton R. N., Mayeda T. K., Olsen E. J. and Goswami J. N. (1991) Oxygen isotope studies of ordinary chondrites. *Geochim. Cosmochim. Acta* **55**, 2317–2337.

Clayton R. N., Onuma N., Grossman L. and Mayeda T. K. (1977) Distribution of the pre-solar component in Allende and other carbonaceous chondrites. *Earth Planet. Sci. Lett.* **34**, 209–224.

Cole D. R. and Chakraborty S. (2001) Rates and mechanisms of isotopic exchange. In *Reviews in Mineralogy & Geochemistry 43, Stable Isotope Geochemistry* (eds. J. W. Valley and D. R. Cole). Mineralogical Society of America, Washington, DC, pp. 83–223.

Connolly, Jr., H. C. and Desch S. J. (2004) On the origin of the "kleine kügelchen" called chondrules. *Chem. Erde Geochem.* **64**, 95–125.

Connolly, Jr., H. C. and Huss G. R. (2010) Compositional evolution of the protoplanetary disk: Oxygen isotopes of type-II chondrites from CR2 chondrites. *Geochim. Cosmochim. Acta* **74**, 2473–2483.

Connolly, Jr., H. C. and Love S. G. (1998) The formation of chondrules: petrologic tests of the shock wave model. *Science* **280**, 62–67.

Cuzzi J. N., Hogan R. C. and Bottke W. F. (2010) Toward initial mass functions for asteroids and Kuiper Belt objects. *Icarus* **208**, 518–538.

Desch S. J., Ciesla F. J., Hood L. L. and Nakamoto T. (2005) Heating of Chondritic materials in solar nebula shocks. In *ASP Conference Series 341, Chondrites and the Protoplanetary Disk* (eds. A. N. Krot, E. R. D. Scott and B. Reipurth). Astronomical Society of the Pacific, San Francisco, CA, pp. 849–872.

Ebel D. S. and Grossman L. (2000) Condensation in dust-enriched systems. *Geochim. Cosmochim. Acta* **64**, 339–366.

Eiler J. M. (2001) Oxygen isotope variations of basaltic lavas and upper mantle rocks. In *Reviews in Mineralogy & Geochemistry 43, Stable Isotope Geochemistry* (eds. J. W. Valley and D. R. Cole). Mineralogical Society of America, Washington, DC, pp. 319–364.

Fagan T. J., Krot A. N., Keil K. and Yurimoto H. (2004) Oxygen isotopic evolution of amoeboid olivine aggregates in the reduced CV3 chondrites Efremovka, Vigarano, and Leoville. *Geochim. Cosmochim. Acta* **68**, 2591–2611.

Fedkin A. V. and Grossman L. (2006) The fayalite content of chondritic olivine: obstacle to understanding the condition of rocky material. In *Meteorites and the Early Solar System II* (eds. D. S. Lauretta and H. Y. McSween Jr.). The University of Arizona Press, Tucson, AZ, pp. 279–294.

Franchi I. A. (2008) Oxygen isotopes in asteroidal materials. In *Reviews in Mineralogy & Geochemistry 68, Oxygen in the Solar System* (ed. G. J. MacPherson). Mineralogical Society of America, Washington, DC, pp. 345–397.

Gounelle M., Krot A. N., Nagashima K. and Kearsley A. (2009) Extreme ^{16}O enrichment in calcium-aluminum-rich inclusions from the Isheyevo (CH/CB) chondrite. *Astrophys. J.* **698**, L18–L22.

Greshake A. (1997) The primitive matrix components of the unique carbonaceous chondrite Acfer 094: A TEM study. *Geochim. Cosmochim. Acta* **61**, 437–452.

Heck P. R., Ushikubo T., Schmitz B., Kita N. T., Spicuzza M. J. and Valley J. W. (2010) A single asteroidal source for extraterrestrial Ordovician chromite grains from Sweden and China: high-precision oxygen three-isotope SIMS analysis. *Geochim. Cosmochim. Acta* **74**, 497–509.

Hezel D. C., Palme H., Brenker F. E. and Nasdala L. (2003) Evidence for fractional condensation and reprocessing at high temperatures in CH chondrites. *Meteorit. Planet. Sci.* **38**, 1199–1215.

Hiyagon H. and Hashimoto A. (1999) ^{16}O excesses in olivine inclusions in Yamato-86009 and Murchison Chondrites and their relation to CAIs. *Science* **283**, 828–831.

Houlier B., Jaoul O., Abel F. and Liebermann R. C. (1988) Oxygen and silicon self-diffusion in natural olivine. *Phys. Earth Planet. Inter.* **50**, 240–250.

Huss G. R., Rubin A. E. and Grossman J. N. (2006) Thermal metamorphism in chondrites. In *Meteorites and the Early Solar Systems II* (eds. D. S. Lauretta and H. McSween Jr.). The University of Arizona press, Tucson, pp. 567–586.

Itoh S., Russell S. S. and Yurimoto H. (2007) Oxygen and magnesium isotopic compositions of amoeboid olivine aggregates from the Semarkona LL3.0 chondrite. *Meteorit. Planet. Sci.* **42**, 1241–1247.

Jabeen I. and Hiyagon H. (2003) Oxygen isotopes in isolated and chondrule olivines of Murchison. *Lunar Planet. Sci.* 34, #1551 (CD-ROM) (abstr.).

Jaoul O., Froidevaux C., Durham W. B. and Michaut M. (1980) Oxygen self-diffusion in forsterite: implications for the high-temperature creep mechanism. *Earth Planet. Sci. Lett.* **47**, 391–397.

Jochum K. P., Stoll B., Herwig K., Willbold M., Hofmann A. W., Amini M., Aaburg S., Abouchami W., Hellebrand E., Mocek B., Raczek I., Stracke A., Alard O., Bouman C., Becker S., Dücking M., Brätz H., Klemd R., de Bruin D., Canil D., Cornell D., de Hoog C.-J., Dalpé C., Danyushevsky L., Eisenhauer A., Gao Y., Snow J. E., Groschopf N., Günther D., Latkoczy C., Guillong M., Hauri E. H., Höfer H. E., Lahaye Y., Horz K., Jacob D. E., Kasemann S. A., Kent A. J. R., Ludwig T., Zack T., Mason P. R. D., Meixner A., Rosner M., Misawa K., Nash B. P., Pfänder J., Premo W. R., Sun W. D., Tiepolo M., Vannucci R., Vennemann T., Wayne D. and Woodhead J. D. (2006) MPI-DING reference glasses for in situ microanalysis: new reference values for element concentrations and isotope ratios. *Geochem. Geophys. Geosyst.* **7**, Q02008.

Jones R. H., Leshin L. A., Guan Y., Sharp Z. D., Durakiewicz T. and Schilk A. J. (2004) Oxygen isotope heterogeneity in chondrules from the Mokoia CV3 carbonaceous chondrite. *Geochim. Cosmochim. Acta* **68**, 3423–3438.

Jones R. H., Saxton J. M., Lyon I. C. and Turner G. (2000) Oxygen isotopes in chondrule olivine and isolated olivine grains from the CO3 chondrite Allan Hills A77307. *Meteorit. Planet. Sci.* **35**, 849–857.

Jones R. H. and Schilk A. J. (2009) Chemistry, petrology and bulk oxygen isotope compositions of chondrules from the Mokoia CV3 carbonaceous chondrite. *Geochim. Cosmochim. Acta* **73**, 5854–5883.

Kimura M., Grossman J. N. and Weisberg M. K. (2008) Fe-Ni metal in primitive chondrites: indicators of classification and metamorphic conditions for ordinary and CO chondrites. *Meteorit. Planet. Sci.* **43**, 1161–1177.

Kimura M., Weisberg M. K., Lin Y., Suzuki A., Ohtani E. and Okazaki R. (2005) Thermal history of the enstatite chondrites from silica polymorphs. *Meteorit. Planet. Sci.* **40**, 855–868.

Kita N. T., Huss G. R., Tachibana S., Amelin Y., Nyquist L. E. and Hutcheon I. D. (2005) Constraints on the origin of chondrules and CAIs from short-lived and long-lived radionuclides. In *Chondrites and the protoplanetary disk* (eds. A. N. Krot, E. R. D. Scott and B. Reipurth). Astronomical Society of the Pacific, San Francisco, CA, pp. 558–587.

Kita N. T., Nagahara H., Tachibana S., Tomomura S., Spicuzza M. J., Fournelle J. H. and Valley J. W. (2010) High precision SIMS oxygen three isotope analyses of UOC chondrules: resolving mass-dependent and mass-independent isotope fractionation. *Geochim. Cosmochim. Acta* **74**, 6610–6635.

Kita N. T., Ushikubo T., Fu B. and Valley J. W. (2009) High precision SIMS oxygen isotope analysis and the effect of sample topography. *Chem. Geol.* **264**, 43–57.

Kobayashi S., Imai H. and Yurimoto H. (2003) New extreme ^{16}O-rich reservoir in the early solar system. *Geochem. J.* **37**, 663–669.

Krot A. N., Hutcheon I. D., Yurimoto H., Cuzzi J. N., McKeegan K. D., Scott E. R. D., Libourel G., Chaussidon M., Aléon J. and Petaev M. I. (2005) Evolution of oxygen isotopic composition in the inner solar nebula. *Astrophys. J.* **622**, 1333–1342.

Krot A. N., Libourel G. and Chaussidon M. (2006a) Oxygen isotope compositions of chondrules in CR chondrites. *Geochim. Cosmochim. Acta* **70**, 767–779.

Krot A. N., McKeegan K. D., Leshin L. A., MacPherson G. J. and Scott E. R. D. (2002) Existence of an ^{16}O-rich gaseous reservoir in the solar nebula. *Science* **295**, 1051–1054.

Krot A. N., Nagashima K., Ciesla F. J., Meyer B. S., Hutcheon I. D., Davis A. M., Huss G. R. and Scott E. R. D. (2010a) Oxygen isotopic composition of the Sun and mean oxygen isotopic composition of the protosolar silicate dust: Evidence from refractory inclusions. *Astrophys. J.* **713**, 1159–1166.

Krot A. N., Nagashima K., Yoshitake M. and Yurimoto H. (2010b) Oxygen isotopic compositions of chondrules from the metal-rich chondrites Isheyevo (CH/CB$_b$), MAC 02675 (CB$_b$) and QUE 94627 (CB$_b$). *Geochim. Cosmochim. Acta* **74**, 2190–2211.

Krot A. N., Yurimoto H., McKeegan K., Leshin L., Chaussidon M., Libourel G., Yoshitake M., Huss G., Guan Y. and Zanda B. (2006b) Oxygen isotopic compositions of chondrules: implications for evolution of oxygen isotopic reservoirs in the inner solar nebula. *Chemie der Erde Geochemistry* **66**, 269–276.

Kunihiro T., Rubin A. E., McKeegan K. D. and Wasson J. T. (2004) Oxygen-isotopic compositions of relict and host grains in chondrules in the Yamato 81020 CO3.0 chondrite. *Geochim. Cosmochim. Acta* **68**, 3599–3606.

Kunihiro T., Rubin A. E. and Wasson J. T. (2005) Oxygen-isotopic compositions of low-FeO relicts in high-FeO host chondrules in Acfer 094, a type 3.0 carbonaceous chondrite closely related to CM. *Geochim. Cosmochim. Acta* **69**, 3831–3840.

Kurahashi E., Kita N. T., Nagahara H. and Morishita Y. (2008) ^{26}Al-^{26}Mg systematics of chondrules in a primitive CO chondrite. *Geochim. Cosmochim. Acta* **72**, 3865–3882.

Libourel G., Krot A. N. and Tissandier L. (2006) Role of gas-melt interaction during chondrule formation. *Earth Planet. Sci. Lett.* **251**, 232–240.

Libourel G. and Chaussidon M. (2011) Oxygen isotopic constraints on the origin of Mg-rich olivines from chondritic meteorites. *Earth Planet. Sci. Lett.* **301**, 9–21.

Maruyama S. and Yurimoto H. (2003) Relationship among O, Mg isotopes and the petrography of two spinel-bearing compound chondrules. *Geochim. Cosmochim. Acta* **67**, 3943–3957.

Maruyama S., Yurimoto H. and Sueno S. (1999) Oxygen isotope evidence regarding the formation of spinel-bearing chondrules. *Earth Planet. Sci. Lett.* **169**, 165–171.

McKeegan K. D., Aléon J., Bradley J., Brownlee D., Busemann H., Butterworth A., Chaussidon M., Fallon S., Floss C., Gilmour J., Gounelle M., Graham G., Guan Y., Heck P. R., Hoppe P., Hutcheon I. D., Huth J., Ishii H., Ito M., Jacobsen S. B., Kearsley A., Leshin L. A., Liu M.-C., Lyon I., Marhas K., Marty B., Matrajt G., Meibom A., Messenger S., Mostefaoui S., Mukhopadhyay S., Nakamura-Messenger K., Nittler L., Palma R., Pepin R. O., Papanastassiou D. A., Robert F., Schlutter D., Snead C. J., Stadermann F. J., Stroud R., Tsou P., Westphal A., Young E. D., Ziegler K., Zimmermann L. and Zinner E. (2006) Isotopic compositions of cometary matter returned by Stardust. *Science* **314**, 1724–1728.

McKeegan K. D., Kallio A. P. A., Heber V. S., Jarzebinski G., Mao P. H., Coath C. D., Kunihiro T., Wiens R. C., Nordholt J. E., Moses, Jr., R. W., Reisenfeld D. B., Jurewicz A. J. G. and Burnett D. S. (2011) The oxygen isotopic composition of the Sun inferred from captured Solar Wind. *Science* **332**, 1528–1532.

McKeegan K. D. and Leshin L. A. (2001) Stable isotope variations in extraterrestrial materials. In *Reviews in Mineralogy & Geochemistry 43, Stable Isotope Geochemistry* (eds. J. W. Valley and D. R. Cole). Mineralogical Society of America, Washington, DC, pp. 279–318.

Myers J. and Eugster H. P. (1983) The system Fe-Si-O: oxygen buffer calibrations to 1,500K. *Contrib. Mineral. Petrol.* **82**, 75–90.

Nagahara H. (1981) Evidence for secondary origin of chondrules. *Nature* **292**, 135–136.

Nagahara H., Kita N. T., Ozawa K. and Morishita Y. (2008) Condensation of major elements during chondrule formation and its implication to the origin of chondrules. *Geochim. Cosmochim. Acta* **72**, 1442–1465.

Nakamura T., Noguchi T., Tsuchiyama A., Ushikubo T., Kita N. T., Valley J. W., Zolensky M. E., Kakazu Y., Sakamoto K., Mashio E., Uesugi K. and Nakano T. (2008) Chondrulelike objects in short-period comet 81P/Wild 2. *Science* **321**, 1664–1667.

Nakashima D., Kimura M., Yamada K., Noguchi T., Ushikubo T. and Kita N. T. (2010) Study of chondrules in CH chondrites – I: oxygen isotope ratios of chondrules. *Meteorit. Planet. Sci. Suppl.* **45**, A148 (abstr.).

Nakashima D., Ushikubo T., Rudraswami N. G., Kita N. T., Valley J. W. and Nagao K. (2011a) Ion microprobe analyses of oxygen three-isotope ratios of chondrules from the Sayh al Uhaymir 290 CH chondrite using a multiple-hole disk. *Meteorit. Planet. Sci.* **46**, 857–874.

Nakashima D., Ushikubo T., Zolensky M. E., Weisberg M. K., Joswiak D. J., Brownlee D. E., Matrajt G. and Kita N. T. (2011b) High precision oxygen three isotope analysis of Wild-2 particles and anhydrous chondritic interplanetary dust particles. *Lunar Planet. Sci.* 42, #1240 (CD-ROM) (abstr.).

Newton J., Bischoff A., Arden J. W., Franchi I. A., Geiger T., Greshake A. and Pillinger C. T. (1995) Acfer 094, a uniquely primitive carbonaceous chondrite from the Sahara. *Meteoritics* **30**, 47–56.

Onuma N., Clayton R. N. and Mayeda T. K. (1972) Oxygen isotope cosmothermometer. *Geochim. Cosmochim. Acta* **36**, 169–188.

Ozawa K. and Nagahara H. (2001) Chemical and isotopic fractionations by evaporation and their cosmochemical implications. *Geochim. Cosmochim. Acta* **65**, 2171–2199.

Pack A., Yurimoto H. and Palme H. (2004) Petrographic and oxygen-isotopic study of refractory forsterites from R-chondrite Dar al Gani 013 (R3.5-6), unequilibrated ordinary and carbonaceous chondrites. *Geochim. Cosmochim. Acta* **68**, 1135–1157.

Rubin A. E., Wasson J. T., Clayton R. N. and Mayeda T. K. (1990) Oxygen isotopes in chondrules and coarse-grained chondrules rims from the Allende meteorite. *Earth Planet. Sci. Lett.* **96**, 247–255.

Rudraswami N. G., Ushikubo T., Nakashima D. and Kita N. T. (2011) Oxygen isotope systematics of chondrules in Allende CV3 chondrite: high precision ion microprobe studies. *Geochim. Cosmochim. Acta* **75**, 7596–7611.

Russell S. D. J., Longstaffe F. J., King P. L. and Larson T. E. (2010) The oxygen-isotope composition of chondrules and isolated forsterite and olivine grains from the Tagish Lake carbonaceous chondrite. *Geochim. Cosmochim. Acta* **74**, 2428–2499.

Russell S. S., MacPherson G. J., Leshin L. A. and McKeegan K. D. (2000) ^{16}O enrichments in aluminum-rich chondrules from ordinary chondrites. *Earth Planet. Sci. Lett.* **184**, 57–74.

Ruzicka A., Hiyagon H., Hutson M. and Floss C. (2007) Relict olivine, chondrule recycling, and the evolution of nebular oxygen reservoirs. *Earth Planet. Sci. Lett.* **257**, 274–289.

Sakamoto N., Seto Y., Itoh S., Kuramoto K., Fujino K., Nagashima K., Krot A. N. and Yurimoto H. (2007) Remnants of the early solar system water enriched in heavy oxygen isotopes. *Science* **317**, 231–233.

Schulze D. J., Harte B., Valley J. W., Brenan J. M. and Channer D. M. R. (2003) Extreme crustal oxygen isotope signature preserved in coesite in diamond. *Nature* **423**, 68–70.

Spicuzza M. J., Day J. M. D., Taylor L. A. and Valley J. W. (2007) Oxygen isotope constraints on the origin and differentiation of the Moon. *Earth Planet. Sci. Lett.* **253**, 254–265.

Steele I. M. (1986) Compositions and textures of relic forsterite in carbonaceous and unequilibrated ordinary chondrites. *Geochim. Cosmochim. Acta* **50**, 1379–1395.

Tenner T. J., Ushikubo T., Kurahashi E., Kita N. T. and Nagahara H. (2011) Oxygen isotopic measurements of phenocrysts in chondrules from the primitive carbonaceous chondrite Yamato 81020: evidence for two distinct oxygen isotope reservoirs. *Lunar Planet. Sci.* 42, #1426 (CD-ROM) (abstr.).

Uesugi M., Sekiya M. and Nakamoto T. (2003) Deformation and internal flow of a chondrule-precursor molten sphere in a shocked nebula gas. *Earth Planets Space* **55**, 493–507.

Ushikubo T., Kimura M., Nakashima D. and Kita N. T. (2010) A combined study of the Al-Mg systematics of O isotope ratios of chondrules from the primitive carbonaceous chondrite Acfer 094. *Lunar Planet. Sci.* 41, #1491 (CD-ROM) (abstr.).

Valley J. W. and Kita N. T. (2009) In situ oxygen isotope geochemistry by ion microprobe. In *Secondary Ion Mass Spectrometry in the Earth Sciences* (ed. M. Fayek). Mineralogical Association of Canada Short Course, 41, Mineralogical Association of Canada, Québec. pp. 19–63.

Wasson J. T., Rubin A. E. and Yurimoto H. (2004) Evidence in CO3.0 chondrules for a drift in the O isotopic composition of the solar nebula. *Meteorit. Planet. Sci.* **39**, 1591–1598.

Weisberg M. K., Ebel D. S., Connolly, Jr., H. C., Kita N. T. and Ushikubo T. (2011) Petrology and oxygen isotope compositions of chondrules in E3 chondrites. *Geochim. Cosmochim. Acta* **75**, 6556–6569.

Weisberg M. K., Ebel D. S., Kimura M., Kita N. T. and Nakashima D. (2010) Petrology and oxygen isotopes of chondrules in the Kota Kota EH3 Chondrite. *Lunar Planet. Sci.* 41, #1756 (CD-ROM) (abstr.).

Wiechert U., Halliday A. N., Lee D.-C., Snyder G. A., Taylor L. A. and Rumble D. (2001) Oxygen isotopes and the Moon-forming giant impact. *Science* **294**, 345–348.

Wood J. A. and Hashimoto A. (1993) Mineral equilibrium in fractionated nebular systems. *Geochim. Cosmochim. Acta* **57**, 2377–2388.

Young E. D. and Russell S. S. (1998) Oxygen reservoirs in the early solar nebula inferred from an Allende CAI. *Science* **282**, 1874–1877.

Young E. D., Ash R. D., Galy A. and Belshaw N. S. (2002) Mg isotope heterogeneity in the Allende meteorite measured by UV laser ablation-MC-ICPMS and comparisons with O isotopes. *Geochim. Cosmochim. Acta* **66**, 683–698.

Yu Y., Hewins R. H., Clayton R. N. and Mayeda T. K. (1995) Experimental study of high temperature oxygen isotope exchange during chondrule formation. *Geochim. Cosmochim. Acta* **59**, 2095–2104.

Yurimoto H., Krot A. N., Choi B.-G., Aléon J., Kunihiro T. and Brearley A. J. (2008) Oxygen isotopes of chondritic components. In *Reviews in Mineralogy & Geochemistry 68, Oxygen in the Solar System* (eds. G. J. MacPherson, D. W. Mittlefehldt, J. H. Jones, S. B. Simon, J. J. Papike and S. Mackwell). Mineralogical Society of America, Washington, DC, pp. 141–186.

Yurimoto H. and Kuramoto K. (2004) Molecular cloud origin for the oxygen isotope heterogeneity in the solar system. *Science* **305**, 1763–1766.

Yurimoto H. and Wasson J. T. (2002) Extremely rapid cooling of a carbonaceous-chondrite chondrule containing very ^{16}O-rich olivine and a ^{26}Mg-excess. *Geochim. Cosmochim. Acta* **66**, 4355–4363.

Zanda B., Bourot-Denise M., Perron C. and Hewins R. H. (1994) Origin and metamorphic redistribution of silicon, chromium, and phosphorus in the metal of chondrites. *Science* **265**, 1846–1849.

Associate editor: Alexander N. Krot